Development, structure, and behavior of a perched lava channel at Kīlauea Volcano, Hawai‘i, during 2007

Tim R. Orr[1], Edward W. Llewellin[2], and Matthew R. Patrick[3]

[1]U.S. Geological Survey, Alaska Volcano Observatory, Anchorage, AK, 99508, USA
[2]Department of Earth Sciences, Durham University, Science Labs, Durham DH1 3LE, UK
[3]U.S. Geological Survey, Hawaiian Volcano Observatory, Hilo, HI, 96720, USA

Highlights

- Detailed description of perched lava channel formed at Pu‘u‘ō‘ō (Kīlauea) in 2007
- Perched lava channel exhibited characteristics of channelized flow and perched lava pool
- Flow lobes exhibited both cooling-limited and volume-limited length controls
- Vesicularity stratification caused vertical variation in flow rheology and velocity
- Seeps of outgassed lava burrowed through and destabilized channel levees

Abstract

Channelized lava flows are commonly produced during the early stages of basaltic eruptions. These channels usually maintain their morphology until the eruption ends or discharge is diverted. In some instances, narrower channels can roof over, developing into lava tubes. We report here on a channelized flow erupted at Kīlauea volcano in 2007 that evolved into a “perched lava channel” composed of a string of interconnected, elongate lava pools, forming a lava channel/lava pool hybrid. The lava channel, which had a time-averaged discharge rate of ~3–9 m^3/s, initially fed a series of flow branches that exhibited cooling-limited and volume-limited controls on flow length, sometimes with each process controlling a different morphological aspect of a single flow branch. The perched lava channel grew vertically primarily by overplating of the channel levees from frequent overflows, forming a compound flow field. This vertical growth only occurred when the distal end of the channel was blocked. When levee failure at the distal end of the channel caused the lava level in the channel to drop below the levee rim, no vertical growth occurred. Seeps of spiny lava and slabby pāhoehoe were common, erupting from uplift scarps on the channel levees, apparently fed by sills from denser, relatively crystal-rich material filling the bottom of the channel. We infer that lava in the channel was stratified in vesicularity and velocity, with foamy, vesicular, faster-moving lava at the top of the lava stream and denser, relatively outgassed, slower-moving lava filling the bottom of the channel. The channel levees were unstable, failing on several occasions, perhaps triggered by the

levee seeps. The appearance of seeps, therefore, is one way of assessing the collapse potential of similar perched lava structures.

Keywords

Hawai‘i, Kīlauea Volcano, Pu‘u‘ō‘ō, eruption, lava channel, perched lava pool

1. Introduction and Field Setting

Kīlauea Volcano’s eruptive activity during 1983–2018 was dominated by discharge from the Pu‘u‘ō‘ō vent, on the volcano’s East Rift Zone (Fig. 1; Wolfe et al., 1988; Heliker and Mattox, 2003; Heliker et al., 2003; Orr et al., 2015b; Orr et al., 2018; Neal et al., 2019), although the volcano also hosted an active lava lake at its summit most of the time during 2008–2018 (Patrick et al., 2021). The Pu‘u‘ō‘ō eruption offered a nearly ideal scenario for studying the evolution and dynamics of a long-lived basaltic eruptive center because of its persistent activity, variety of eruptive styles and behaviors, and relative ease of access. The eruption was characterized during the first three years by episodic lava fountains and pyroclastic cone construction, but activity transitioned to nearly continuous effusion in 1986. It was distinguished thereafter by shield construction and tube-fed lava flows, interrupted occasionally by brief fissure eruptions nearby.

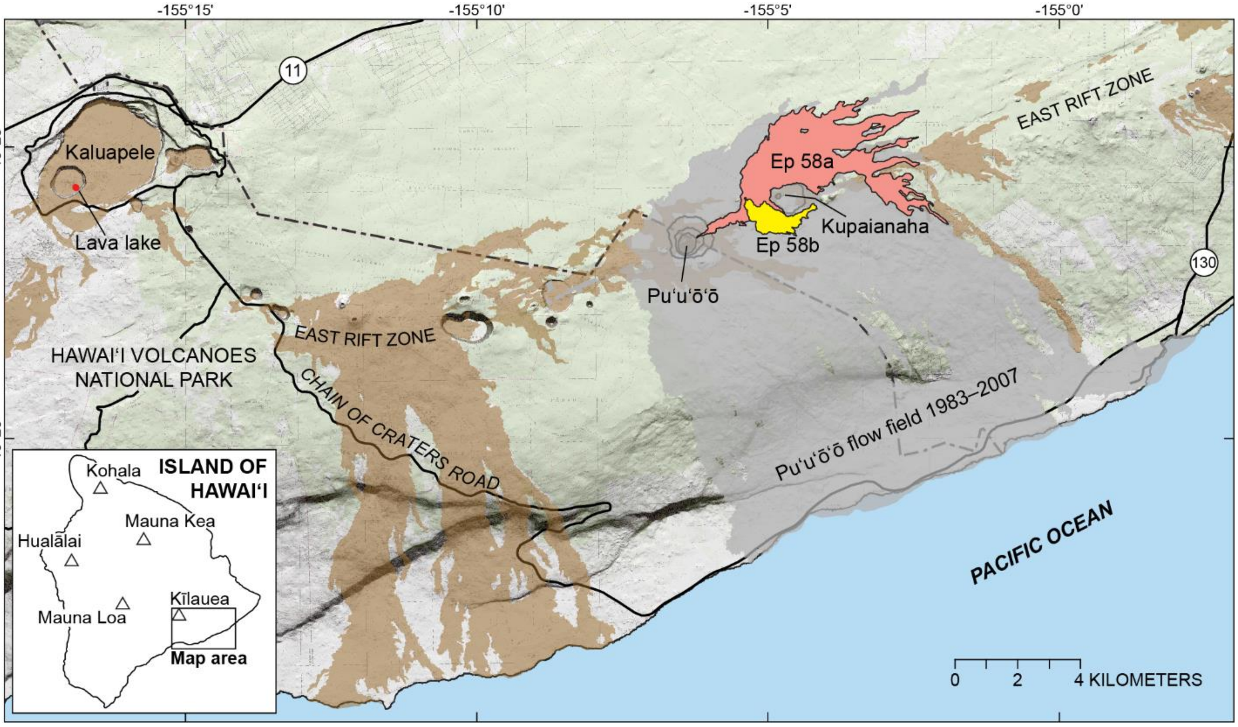

Figure 1. Map of Kīlauea’s summit and East Rift Zone. Historical lava flows 1790–1979 in brown; lava flows from Pu‘u‘ō‘ō eruption January 1983–June 2007 in gray; episode 58a of the Pu‘u‘ō‘ō eruption July–December 2007 in red; episode 58b of the Pu‘u‘ō‘ō eruption November–December 2007 in yellow. (Inset): Map of Hawai‘i showing Figure 1 map area.

The Puʻuʻōʻō eruptive sequence comprised 62 episodes, based loosely on eruptive style and vent location. The episode nomenclature was used inconsistently during the eruption, but nonetheless provides a convenient way of conveying chronological information about this long-lived eruption. Some episodes were further divided into sub-episodes identified with letter designations. Informal names, often date- or holiday-based, were also commonly used in addition to the episode and sub-episode designations.

In this paper, we document a critical change in the Puʻuʻōʻō eruption—the beginning and early evolution of a new episode of eruptive activity—that spanned July–December 2007. This started with the opening of a new vent on the northeast flank of the Puʻuʻōʻō cone and the eruption of a channelized lava flow, which in time built a compound flow field (Walker, 1971). This activity, which was designated episode 58a of the eruption, came towards the end of a 4-year period (2003–2007) during which the magma supply rate to Kīlauea was more than double the multi-decadal background supply rate (Poland et al., 2012).

The early part of the Episode 58 eruption saw the emplacement of a series of simple, channelized lava flows. Such flows, unless they encounter a topographic barrier, are controlled either by (1) viscosity and yield strength, as regulated by heat loss (cooling-limited), which is related in turn to eruption rate, or by (2) the supply of material erupted (volume-limited), which is related to eruption duration (e.g., Walker et al., 1973; Malin, 1980; Pinkerton and Wilson, 1994; Harris and Rowland, 2009). Both factors played a role during episode 58a, sometimes with competing influences on the same flow lobe.

As the flow field developed, channelized flows were superseded by the development of an unusual hybrid between a perched lava pool and a lava channel—a “perched lava channel”. This feature eventually stood as much as 45 m above the pre-2007 flow surface, forming a string of four perched lava pools when viewed in profile but maintaining a channel-like morphology in map view. We present here a detailed description and discussion of eruptive activity during episode 58a. Specifically, we look at the controls on run-out length of flow lobes, the evolution of a channelized flow into a perched lava channel, the self-repair of channel breaches, effusion rate estimates, the extrusion of spiny lava and slabby pāhoehoe seeps from the lower flanks of the channel levees, the destabilization and failure of levees, and density and velocity stratification of the lava stream.

We use the descriptive term “lava pool” to refer to all pond-like accumulations of lava, impounded by levees, that formed during this period of the eruption. The spellings of the Hawaiian place names used here are as currently prescribed by the United States Board on Geographic Names.

2. Data Collection

This paper is based primarily on field observations conducted during helicopter overflights, which occurred generally every 2 to 3 days and typically included time on the ground. The study area was also monitored by a telemetered webcam and by time-lapse cameras that stored imagery locally. The resulting images supplement direct field observations and are used to quantify channel growth and behavior. Camera parameters are detailed in Patrick et al. (2011).

Flow margins were typically mapped using a hand-held GPS by flying along the outermost perimeter of the flow during helicopter overflights. The GPS track log collected in this fashion during each overflight was incorporated into previous mapping to generate regularly updated flow outlines. Internal flow contacts were not mapped. In rare cases, portions of the flow margin were mapped on the ground using a hand-held GPS, with an accuracy of ±10 m. Contacts mapped from the air are generally accurate to within ±30 m, based on direct comparison between contacts mapped using both techniques. The accuracy of the aerial mapping in some areas, however, for example at tight corners not navigable by helicopter, could be ±50 m.

Topographic data were collected in early October 2007, during a period when overflows from the perched channel were absent, by walking a series of transects across the flow with a backpack-mounted kinematic GPS. The vertical accuracy of this method through repeated use at the Hawaiian Volcano Observatory has been found to be ±20 cm—greater than the errors introduced by a person's gait during walking. GIS software was used to create a digital terrain model (DTM) from the kinematic GPS data. Differencing of the newly constructed DTM with the pre-event 2005 Hawaii IFSAR DTM allowed an approximate flow volume to be calculated. Because most of the volume comprised ʻaʻā flows, bulk volume was converted to dense-rock equivalent (DRE) volume by assuming 25% void space (Wolfe et al., 1988).

The vertical growth of the four pools that composed the perched channel was determined from a webcam on the upper north flank of Puʻuʻōʻō that recorded images at 1-minute intervals. Image resolution is 640×480 pixels. The webcam's angular field of view was calculated to be 9.47º using geographic features in the image and their distance from the webcam, both measured from satellite imagery using GIS software. The distance from the webcam to each of the four pools along fixed vectors was also measured using GIS software. With these parameters, the respective pixel size in meters at each pool was determined (Pool 1 = 0.635 m, Pool 2 = 0.693 m, Pool 3 = 0.733 m, Pool 4 = 0.769 m). The height of the pools in pixels was then measured at a fixed x-position for each pool over the duration of the eruption and converted to meters to get the height of the channel above the pre-2007 flow surface. These values were calibrated using the topographic data collected in October. The noise in the measurements indicates an error of about ±2 m.

Calculating the local dense-rock-equivalent volume flux of lava flowing through the channel requires three parameters—mean lava stream velocity, cross-sectional area of the stream, and vesicularity of the lava. (1) The surface velocity of the channelized lava stream was determined on the ground and from webcam imagery by timing the transit of features near the center of the lava stream between points on the channel rim. Mean velocity was then calculated by multiplying the surface velocity by 0.67 to account for horizontal and vertical velocity variations (Harris et al., 2007); this carries the assumption that the lava has uniform Newtonian rheology and corresponding parabolic velocity profile. (2) The cross-sectional area of the lava stream was determined by multiplying width by depth, assuming a rectangular cross section based on observations of the channel after it was abandoned. Channel width was measured from georegistered aerial imagery using GIS software. Minimum channel depth was measured by dropping steel construction rebar into the lava channel from the belly hook of a helicopter hovering high above the channel, as well as from laser rangefinder measurements of channel depth after it was abandoned. The rebar was 6 m long with 2 m of cable attached to one end (total length 8 m). We use levee height as a proxy for maximum channel depth (e.g., Calvari et al. 2003). (3) The density of the lava in the channel was calculated from 3–5 cm diameter pieces of overflow crust using Archimedes' Principle following the approach of Houghton and Wilson (1989) and using wax film. Density was converted to vesicularity using a dense-rock-equivalent density of 2.75 g/cm^3 (Lesher and Spera, 2015). We collected the clasts in 2021, in discrete locations <10 m from the rim of pools 1 (80 clasts), 3 (65 clasts), and 4 (63 clasts). We also analyzed the vesicularity of two seeps that extruded through the perched channel levee at pool 4, using 10 clasts collected in 2013 and 20 clasts collected in 2021.

3. Field Observations and Measurements

The evolution of the flow field produced by the episode 58a eruption was captured via routine mapping and field observations throughout the eruption. Fig. 2 presents a series of maps showing the evolution of the flow field, including the location of the main perched channel and major breakout channels, within the broader context of the pre-existing topography. Table 1 divides the activity into eight phases based primarily on vertical levee growth (Fig. 3), presenting an overview of the chronology of the eruptive activity we discuss. The eight panels of Fig. 2 map onto the 'phases' of the eruption identified in Table 1.

161

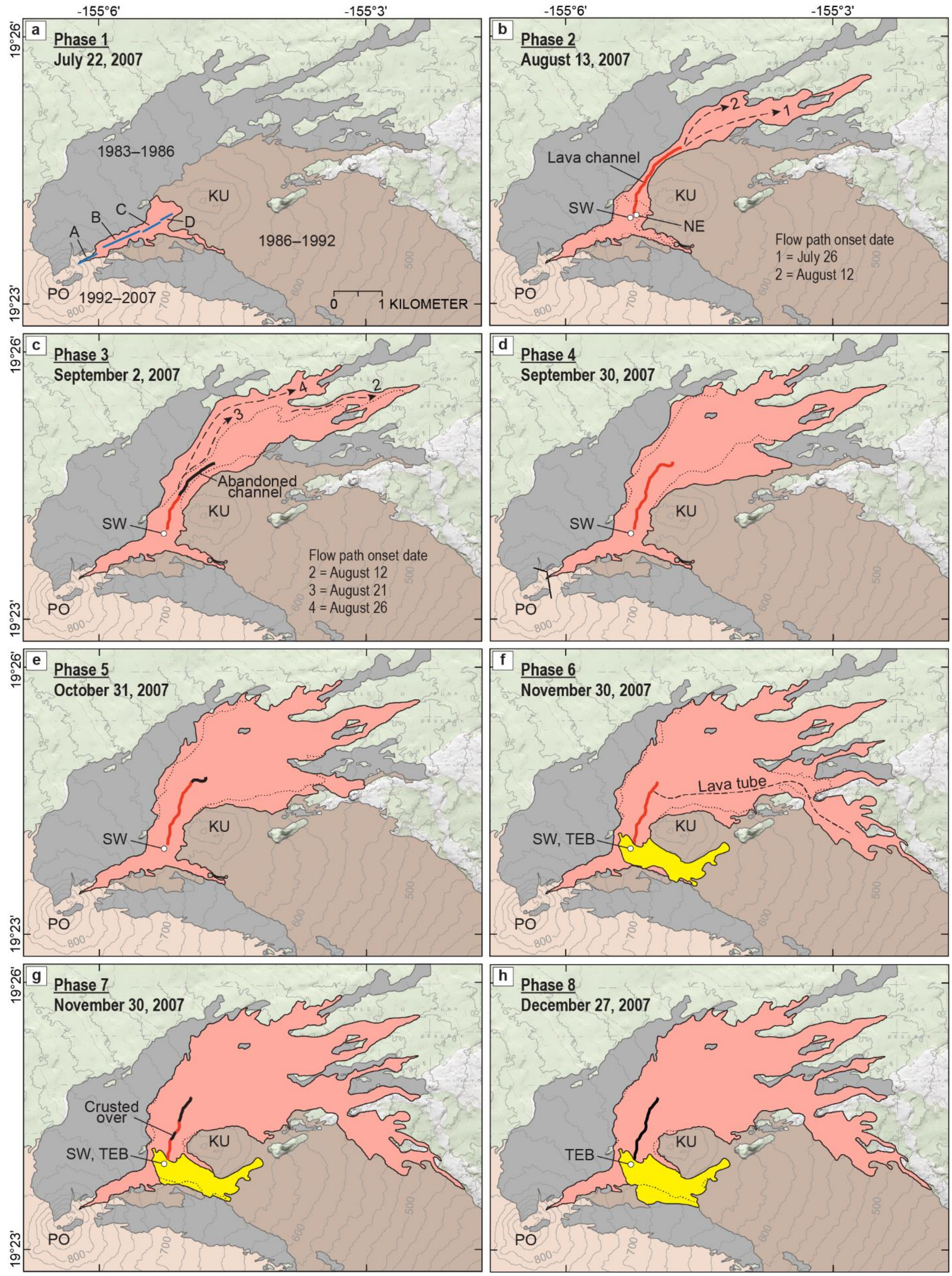
-155°6'
-155°3'
19°26'
19°23'
a
Phase 1
July 22, 2007
1983–1986
KU
A
B
C
D
1986–1992
PO
1992–2007
0
1 KILOMETER
b
Phase 2
August 13, 2007
Lava channel
SW
NE
Flow path onset date
1 = July 26
2 = August 12
c
Phase 3
September 2, 2007
Abandoned channel
Flow path onset date
2 = August 12
3 = August 21
4 = August 26
d
Phase 4
September 30, 2007
e
Phase 5
October 31, 2007
f
Phase 6
November 30, 2007
Lava tube
SW, TEB
g
Phase 7
November 30, 2007
Crusted over
h
Phase 8
December 27, 2007
TEB

Figure 2. Maps of episode 58 flow field showing eruptive fissures (blue lines) and active vents (white circles), selected flow paths with onset dates (dashed black lines; 1 = July 26, 2 = August 12, 3 = August 21, 4 = August 26), perched lava channel (red line = active; black line = abandoned), and evolution of episode 58a (light red) and 58b (yellow) flow fields on dates indicated. Each map is a snapshot of the flow field during eruptive phases shown in Table 1. Dotted black lines show flow extent from previous map panel; PO is Pu‘u‘ō‘ō; KU is Kupaianaha; SW is vent at southwest end of fissure D; NE is vent at northeast end of fissure D; TEB is Thanksgiving Eve Breakout vent, same location as SW vent.

Table 1. Chronology of perched channel evolution.

Phase 1	July 21–28 Fig. 2a	Initial lava emplacement lays foundation for channel.
Phase 2	July 28–August 20 Fig. 2b	Unrestricted flow through channel. Distributary field grows. No significant vertical growth.
Phase 3	August 20–September 14 Fig. 2c	Channel blockages cause backups, overflows, and levee construction, enabling vertical growth and creating pools, which we number 1 (most proximal) to 4 (most distal). Levees reach 20–35 m in height. Average vertical growth rates: pool 1 = 0.5 m/day, pool 2 = 0.8 m/day, pool 3 = 0.9 m/day, pool 4 = 0.9 m/day.
Phase 4	September 14–October 13 Fig. 2d	Unrestricted flow through channel. Cascade at distal end of pool 4 feeds into lower channel. No significant vertical growth except at lower channel. Kinematic GPS survey conducted during this period.
Phase 5	October 13–November 6 Fig. 2e	Lower channel crusts over; outflow from pool 4 restricted. Lava backs up and overflows, causing renewed vertical growth. Levees reach 30–45 m in height. Average vertical growth rates: pool 1 = 0.4 m/day, pool 2 = 0.5 m/day, pool 3 = 0.5 m/day, pool 4 = 0.4 m/day.
Phase 6	November 6–December 4 Fig. 2f	Efficient flow through pool 4 SE tube. Lava level drops ~10 m on November 21 due to onset of new vent-proximal flow: Thanksgiving Eve Breakout (TEB) flow. No significant vertical growth. Channel inactive by November 30.
Phase 7	December 4–17 Fig. 2g	Lava returns to pools 1 and 3 during first week of December, feeding vigorous overflows and developing extensive pool 3 seep terraces. Pools 1 and 3 build vertically by an additional 4–7 m; pools 2 and 4 no longer host active lava (tube develops within crusted-over pool 2, connecting pools 1 and 3).
Phase 8	December 17–31 Fig. 2h	Lava below channel rim for several days, and then channel abandoned. Pool levees begin to break down, partially filling emptied pools with rubble. TEB flow captures all discharge.

3.1 Eruption onset and relationship to pre-existing topography

Episode 58a began with the opening of four fissure segments—designated A to D from west to east—on the northeast flank of Pu‘u‘ō‘ō (Figs. 2a, 4a). The fissure segments opened over the course of a few hours, propagating downrift (and downslope). The fissure system extended a total length of 2.12 km, from an elevation of 835 m at its southwest tip on the flank of Pu‘u‘ō‘ō (around 110 m from the crater rim) to an elevation of 695 m at its northeast tip in the saddle between Pu‘u‘ō‘ō and Kupaianaha.

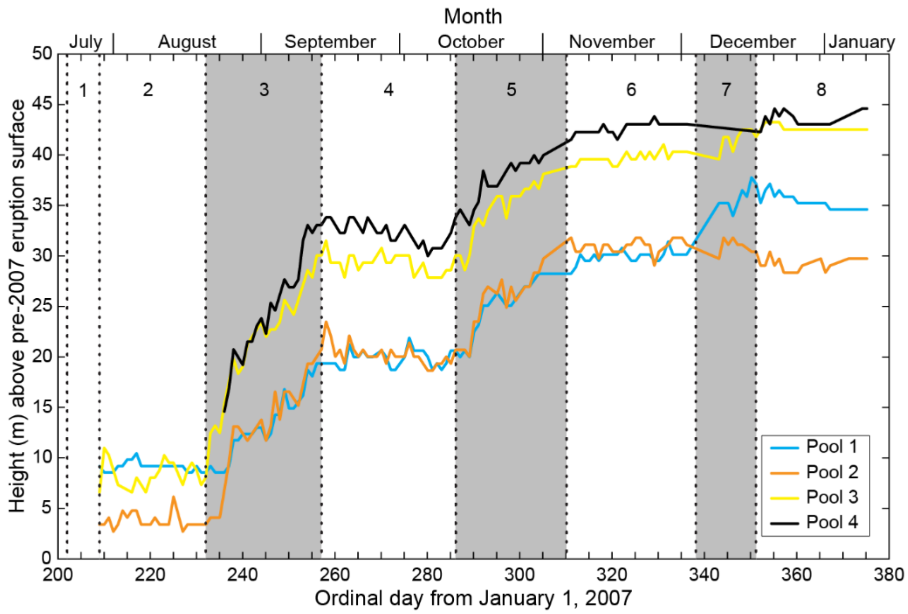

Figure 3. Graph showing vertical growth history of perched lava channel measured from webcam imagery (Section 2). Colored lines represent vertical growth, in meters above pre-emplacement surface, of each of the four pools. Distinct phases of growth (gray bars), separated by phases of little or no growth, are readily apparent (labeled 1–8; see Table 1). Phase 1 preceded preceded formation of perched lava channel.

Phase 1 (Fig. 2a) was characterized mostly by channelized pāhoehoe flows that followed the axes of the fissures and then spread up to a few hundred meters away from the fissures on both sides. Localization of activity over portions of the fissures led to accumulation of lava over discrete parts of fissures B, C, and D, forming lobate perched lava pools that developed through repeated overflow and levee construction at the most dominant of the early-formed channels. Episodic failure of the flanks of the perched pools fed ʻaʻā flows that, initially, broadened the lava flow field on both sides of the fissure, then focused toward the northeast—the path that eventually formed the persistent perched channel that is our main focus. These flows were emplaced on a 1–2^{o} slope, within a broad valley, confined to the south by the north flank of Kupaianaha and to the north by older Puʻuʻōʻō ʻaʻā flows (Figs. 2, 4b–d).

3.2 Channel formation

The channel that would become the perched channel formed via a series of four breakouts over the course of a month spanning from late Phase 1 to early Phase 3 (Figs. 2b, 2c); each flow was named for the date on which the breakout occurred. The channel was first established by a major breakout triggered by the failure of the flank of the perched pool that developed over fissure D. This breakout fed the “July 26” flow (Figs. 2b, 4b, 4c), which advanced at a time-averaged rate of about 30 m/hr. The flow was channelized for the first 1.8 km, and then transitioned into a clinkery ʻaʻā flow (the zone of dispersed flow; Lipman and Banks, 1987; Fig. 4c), which subsequently stalled about 3.7 km from the vent. Beyond this point, lava was conveyed to the flow front through the molten core of the ʻaʻā flow, perhaps through an incipient lava tube system, and emerged from the sides and front of the distal ʻaʻā flow as sluggish breakouts of spiny lava and slabby pāhoehoe (Rowland and Walker, 1987; Harris et al., 2016; Fig. 4c).

Despite the change in advance rate and texture, the flow continued to move forward and broaden significantly (up to 825 m across) and eventually reached a length of ~6 km.

Slowing of the clinkery ‘a‘ā at the front of the “July 26” flow caused lava to back up in the channel and feed overflows of shelly pāhoehoe that buried the initial ‘a‘ā levees (Sparks et al., 1976). The north side of the channel failed while the channel was full, near the transition to dispersed flow, cutting off supply to the “July 26” branch, which soon stalled. The breakout from the failure point fed a new ‘a‘ā flow branch, the “August 12” flow, which hugged the north margin of the “July 26” branch (Figs. 2b, 2c, 4d). This flow branch also began to produce spiny lava and slabby pāhoehoe from its front and sides as it approached its terminal length.

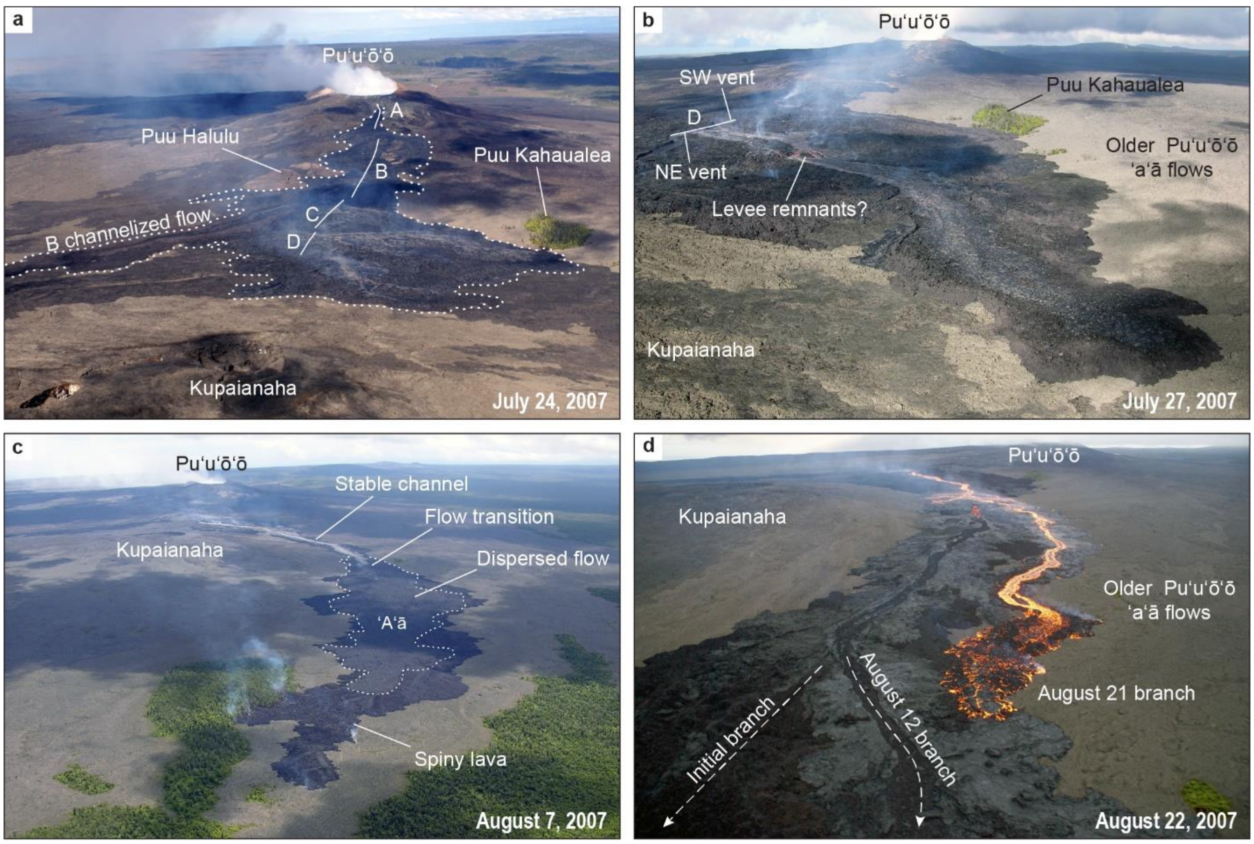

Figure 4. (a) Fissures A–D (solid white lines) and episode 58a lava flow (dotted white outline) three days after eruption onset, looking west-southwest. Perched lava pools beginning to form over fissures C and D. Fissure B feeding channelized flow to southeast. Photograph by J. Kauahikaua, U.S. Geological Survey, July 24, 2007. (b) Early development of fissure D channelized flow, looking west-southwest. Flow probably initiated by failure of perched lava pool levee. Flow fed by two distinct points of effusion near northeast (NE) and southwest (SW) ends of fissure D. Photograph by T. Orr, U.S. Geological Survey, July 27, 2007. (c) Channelized flow, looking west-southwest, showing transition between the stable channel and zone of dispersed flow. Boundary between initial ‘a‘ā flow and later spiny lava and slabby ‘a‘ā marked with dotted white line. Photograph by T. Orr, U.S. Geological Survey, August 7, 2007. (d) “August 21” flow branch traveling along north edge of abandoned channel, having cut off supply to the “August 12” flow branch. The “August 12” flow previously cut off supply to initial “July 26” channelized flow. Photograph by J. Kauahikaua, U.S. Geological Survey, August 22, 2007.

Supply to the “August 12” branch of the flow was cut off nine days later, when the channel developed a blockage about 850 m from the vent and began to overflow. The “August 12” flow channel downstream from the blockage was subsequently abandoned (Fig. 4d). Lava spilling from the channel at the blockage fed another channelized ‘a‘ā flow—the “August 21” flow—that traveled along the north margin of the “August 12” flow for the next few days (Fig. 4d). Lava supply to the “August 21” flow branch soon waned, however, as lava began to accumulate in the upstream part of its channel, just downstream from the diversion caused by the blockage of the “August 12” flow. The accumulation of lava constructed an elongate perched lava pool that eventually became a new part of the stable channel, which thereafter had a length of ~1.4 km. The northern flank of the filled and overflowing perched lava pool failed within a few days, feeding another ‘a‘ā flow lobe—the “August 26” flow—along the north margin of the previously emplaced flows (Fig. 2c). The “August 26” flow branch stalled around a week later as the end of the stable channel became progressively blocked, and the supply of lava feeding the flow branch waned.

3.3 Development of the perched channel

Phase 3 was characterized by rapid growth (above the pre-eruption surface) of the levees of the channel that was established during Phase 2 (Fig. 3). Overflows of shelly pāhoehoe from the channel became more common during Phase 3 (Fig. 5a) as the more distal flow field was progressively buried by ‘a‘ā flows and the added thickness prevented lava from easily exiting the channel. The frequent overflows caused lava to accumulate on the channel levees, which, in turn, caused the levees to grow vertically. Growth was augmented by draping of rafted plates of surface crust from lava in the channel onto the levees (Fig. 5b). The vertical growth of the levees caused the channel to become distinctly perched above the surrounding landscape, forming a long ridge (Figs. 5c, 5d, 6). As the channel levees became more elevated and the channel deepened, the gradient and velocity of the lava stream decreased, which resulted in even more overflows. It was during Phase 3 that the lava channel also began to acquire the general shape—the bends, constrictions, and swells—that it retained thereafter (Figs. 5c, 5d). Channel overflows during lava level high-stands (Fig. 5a) caused the narrowest parts of the lava channel to narrow further and crust over, segmenting the channel into a string of four distinct pools, which we call pools 1–4, with pool 1 closest to the vent (Figs. 5a, 5c, 5d). This distinctness was maintained even when the bridges were not present and the pools were separated by narrow sections of channel.

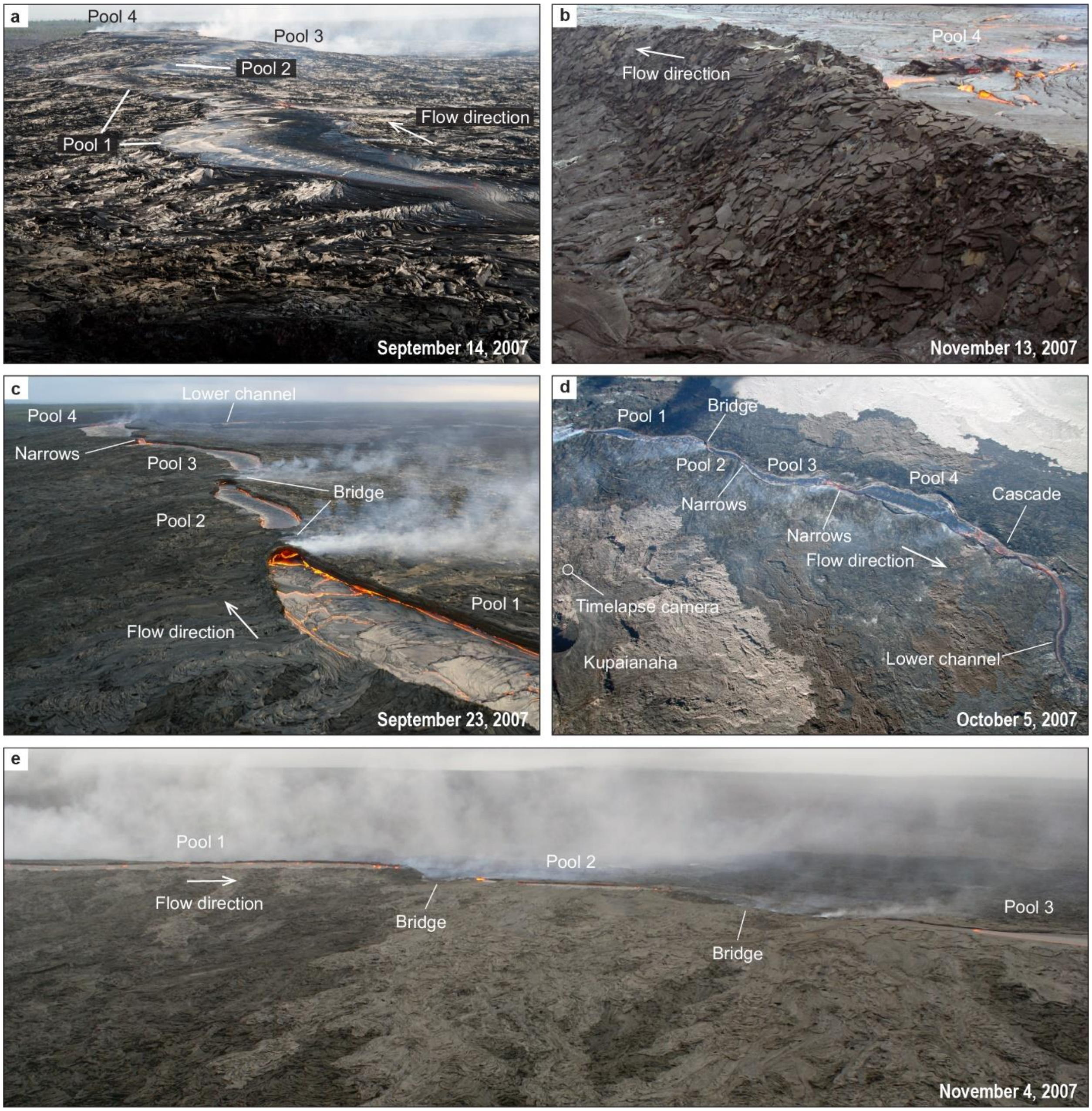

Figure 5. (a) Perched lava channel full and overflowing along nearly entire length. View to the northeast. Photograph by T. Orr, U.S. Geological Survey, September 14, 2007. (b) Imbricated plates of rafted surface crust mantling levee on north side of pool 4. Photograph by J. Kauahikaua, U.S. Geological Survey, November 13, 2007. (c) Pools 1–4 of perched channel. Bridges formed during high stands present between pools 1, 2, and 3. Narrow rapids separate pools 3 and 4. Lava empties from pool 4 down steep ramp into lower channel in distance. Photograph by J. Kauahikaua, U.S. Geological Survey, September 23, 2007. (d) View of perched channel showing pools 1–4 and lower channel. Photograph by T. Orr, U.S. Geological Survey, October 5, 2007. (e) Bridges over channel between pools led to different vertical growth history for each, giving perched channel a stair-stepped appearance in profile from pool to pool. Bridges formed saddles lower than pool on either side. Photograph by J. Kauahikaua, U.S. Geological Survey, November 4, 2007.

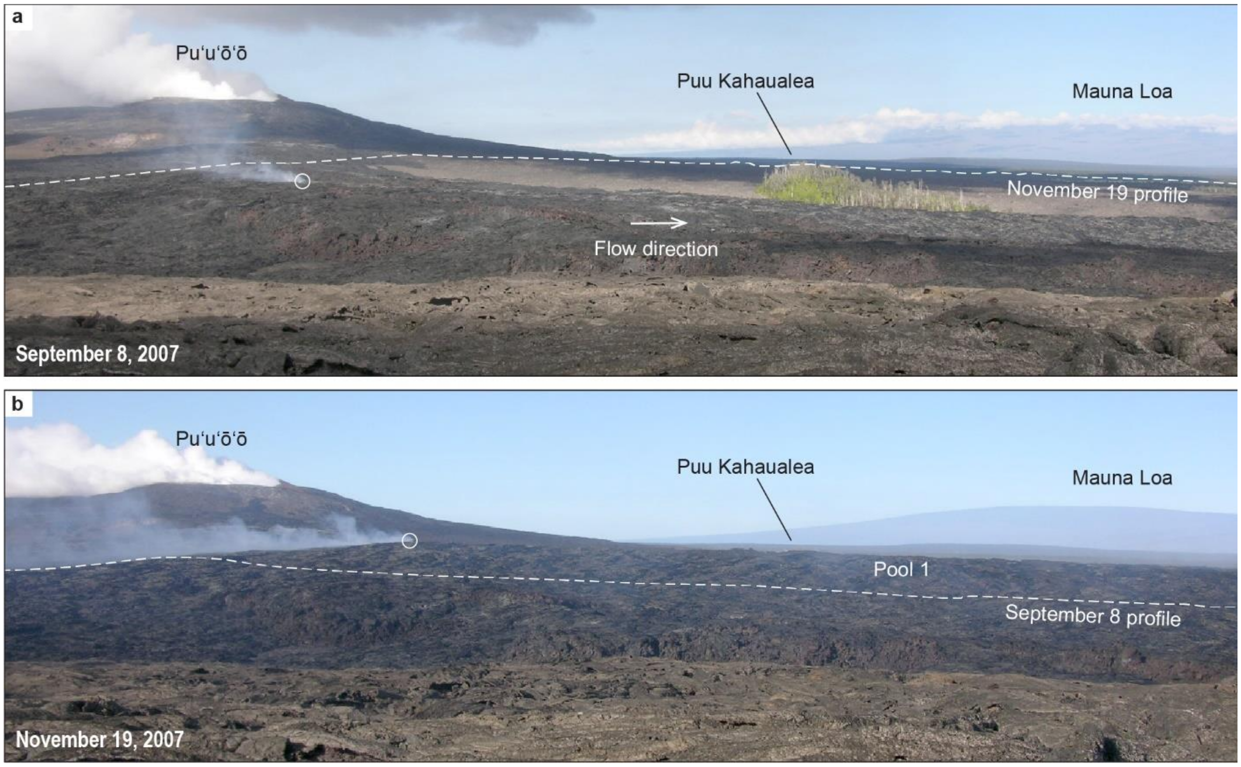

Figure 6. Time-lapse camera views looking west on (a) September 8, 2007, and (b) November 19, 2007, showing vertical growth of perched lava channel. White circles markproximal end of pool 1 (. Dashed white lines illustrate change to channel profile. Camera location shown in Fig. 5d.

3.4 Structure and geometry of the perched channel

In their final form (Fig. 7a), the lengths of the pools were 410 m (pool 1), 85 m (pool 2), 220 m (pool 3), and 400 m (pool 4). These lengths are based on imagery collected in 2010, well after episode 58a ended—the pools were mostly buried by 2016. Pools 1–3 had relatively simple shapes—the width of pool 1 generally ranged from 35 to 45 m, pool 2 was 15–25 m across, and pool 3 was 15–40 m across. In comparison, pool 4 was more variable in width, probably because it was the site of repeated levee failures. It ranged from about 20 to 90 m across.

The channel built vertically during periods of overflow (principally phases 3, 5, and 7) and was approximately rectangular in cross section, based on observations after the perched channel was abandoned (Fig. 8). An analysis of time-lapse imagery shows that, over the duration of Phases 3–5, the channel built upward at an average rate of ~0.3 m/day. In detail, though, the vertical growth was unsteady (Fig. 3), occurring only during periods of overflow (Table 1). Video 22 of Orr (2011) is a time-lapse movie showing vertical growth of pool 1 from September 8 to November 30, 2007 (https://pubs.usgs.gov/ds/621/2007/22_Ep58PerchedChannelGrowth_8Sep-30Nov2007/). By Phase 8, the levees of pools 1, 2, 3, and 4 were approximately 35, 30, 43, and 45 m, respectively, above the pre-July 2007 surface based on webcam and theodolite measurements. The outer slopes of the levees were generally 4–5º, although parts of the pool 4 levee close to the channel rim were too steep to walk up (e.g., Fig. 5b).

Overflows from the channel resulted in shelly pāhoehoe, which contained hot cavities a meter or more deep. The thickness of the crust composing the shells increased from 3–4 cm at pool 1 to

10–15 cm at pool 4. Samples of the surface crust of overflows were collected after the eruption had finished and were analyzed to determine vesicularity (Fig. 7b, 7c, 7d). The average vesicularity of the surface crust of overflows from pools 1, 3, and 4 is 0.73 (range 0.65–0.79), 0.71 (range 0.59–0.79), and 0.60 (range 0.49–0.69) respectively (Fig. 7e).

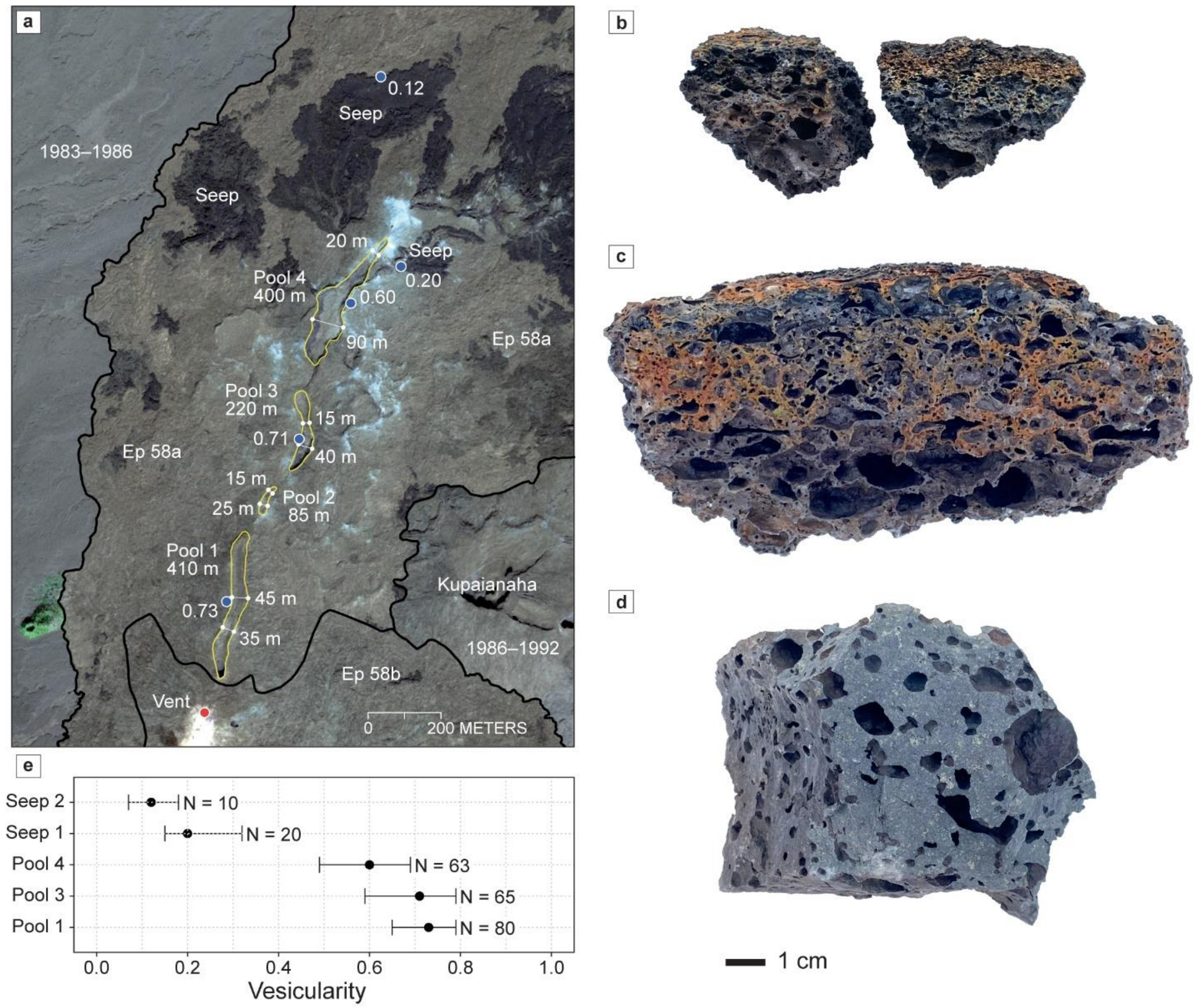

Figure 7. (a) Map showing final form of the four perched channel pools (yellow outlines), along with their lengths and widths, after Episode 58a had ended. Blue circles show sample locations and average vesicularity. Red circle shows the location of vent that fed perched channel. Base acquired December 12, 2010. DigitalGlobe, NextView license. (b) Photograph showing pieces of overflow crust collected at pool 1. Crust thickness is 4 cm. (c) Photograph showing piece of overflow crust at pool 4. Crust thickness is 8 cm. (d) Photograph showing rock sample from a seep north of pool 4. (e) Plot showing sample vesicularity and number of clasts measured. Black circle corresponds to average vesicularity; bar marks minimum and maximum vesicularity for each sample set.

The depth of the channel was estimated in three ways. First, the depth was estimated during Phase 4 by dropping rebar from a helicopter into pool 2 and into the lower channel below pool 4. At pool 2, ~500 m downstream from the vent, where the channel was ~20 m wide, the rebar spear struck the center of the channel and completely disappeared (including the cable tail), suggesting a depth exceeding 8 m. At the time of the measurement, the levee stood ~20 m above the pre-2007 land surface (Fig. 3) and the lava surface was about 2 m below the channel rim, indicating a maximum channel depth of 18 m, assuming the channel had not cut down into the pre-eruption surface. At the lower channel ~1.5 km downstream from the vent, where the channel was 17 m wide, a rebar spear hitting near the center of the channel indicated a depth of ~2 m. Second, the depth of the drained channel was measured during Phase 8, finding the floor of pool 1 to be as much as 16.5 m below the levee rim. This is a minimum channel depth because the pool was floored by rubble and a residual crust after it drained. (Fig. 8). Third, rapid changes in lava depth allowed minimum lava depths to be estimated on a few occasions. During Phase 4, the lava level dropped at least 6 meters along the length of the channel and then recovered, with no obvious cause. During Phase 6, the onset of the Thanksgiving Eve Breakout (TEB) flow caused the lava level in pool 1 to drop by 10 m; at the same time the maximum depth based on levee height was ~30 m (Fig. 5).

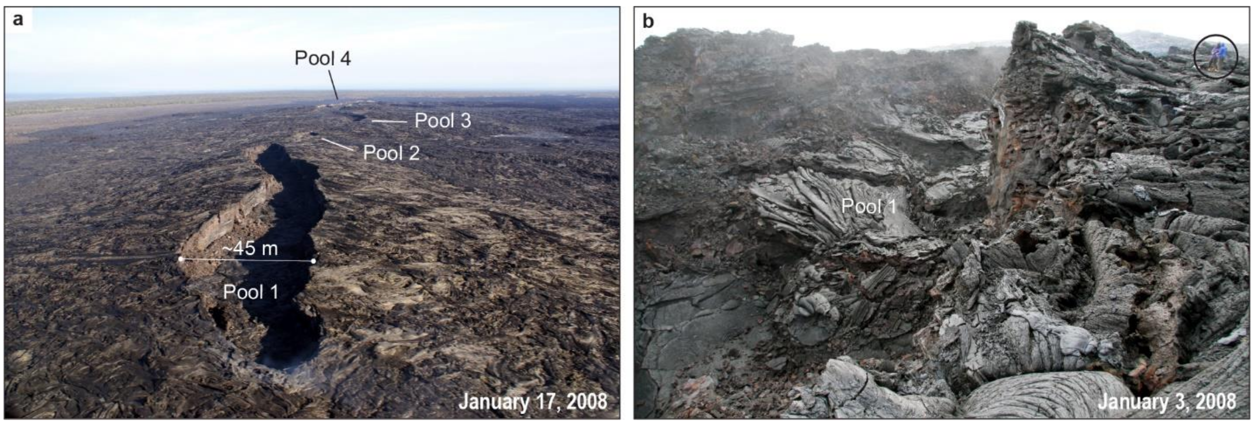

Figure 8. (a) Abandoned perched channel pools 1–4. Photograph by J. Kauahikaua, U.S. Geological Survey, January 17, 2008. (b) Abandoned perched channel pool 1. Geologists at upper right (circled) for scale. Photograph by T. Orr, U.S. Geological Survey, January 3, 2008.

Between the pools, the channel was sufficiently narrow that it crusted over across its full width at times, forming lava bridges (Figs. 5c, 5d). During Phase 3, these bridges formed between pools 1, 2 and 3, and briefly between pools 3 and 4. At the start of Phase 4, a levee collapse at the downstream end of pool 4 produced a persistent outlet that resulted in a lava level generally 2–3 m below the channel rim in all pools, leading to the collapse of the lava bridges. During Phase 5, vertical growth of the levees of the channel below pool 4 elevated it almost to the level of the main perched channel causing the upper channel to refill, overflow its levees, and resume its vertical growth (Fig. 3). These changes were accompanied by the stagnation and crusting over of the lower channel, which was gradually abandoned. New bridges soon grew at the constrictions between pools 1–4, and elevation differences from one pool to the next produced a distinct downstream stair-stepped appearance when viewed in profile (Fig. 5e). By Phase 7, only pools 1 and 3 hosted lava and occasional overflows. Pool 2 hosted no surface activity, though lava traveled beneath its crusted surface through a lava tube that connected pools 1 and 3. Pool 4 was inactive.

3.5 Behavior of the perched channel

Quantitative on-site measurements of channel velocity were only made on one occasion, in October when the lava stream was below the channel rim. At pool 2, the surface velocity was 0.5 m/s, while in the lower channel below pool 4, where the gradient was slightly steeper, the velocity was 1.1 m/s. The surface velocity of pool 1 during November 15–17, based on webcam imagery, averaged 0.18 m/s (Patrick et al., 2011). In general, the stream velocity increased as channel width decreased—for example, at the narrower constrictions between the pools.

Large blocks of solidified lava, as much as 5 m (or more) across, were observed to travel slowly down the channel at times. These blocks, which were probably equivalent to the "lava boats" observed by Lipman and Banks (1987) in channels during the 1984 Mauna Loa eruption, were observed only during times of low lava level in the channel, and only near the outlet of pool 4. The blocks traveled much more slowly than the surface of the lava stream (meters per hour, compared with 10s of cm per second). None were observed to roll, though observations were sparse, but it seems reasonable that some blocks could have moved in that fashion, at least at times. During Phase 4, when lava cascaded from pool 4 down a gentle incline into a lower channel, blocks 3–5 m across were observed up close sliding down the cascade. Each block partly obstructed the lava stream, which formed a bow wave on the upstream side of the blocks that sometimes overtopped them. Near the base of the incline, the velocity of one of the blocks was measured at ~1 m/min, and it slowly submerged as it slid into the lower channel, which apparently deepened. Islands of crust were observed in the lower half of pool 4 during periods of low lava level, which may have formed over submerged blocks. These islands seemed stationary but were observed to have moved downstream on the few occasions when observations were made a few hours apart. None of the islands or blocks persisted over the period between field visits.

The surface of the lava in the channel had a lumpy appearance in the most vent-proximal part of pool 1, apparently formed by doming of a flexible crust over gas pockets and at times the surface of the lava stream stood a few 10s of cm higher than the channel rim, from which it was separated by a shear zone along both sides of the channel (Fig. 9a). The gas pockets were transitory, losing their contents by continued outgassing or when the domed crust ruptured, and were far smaller and less prevalent in the lower stretches of pool 1 and in the other pools. Instead, the channel surface there was topped by a crustal sheet characterized by large arcuate folds with the convex side facing downstream. In pool 4, which varied more in width, the crust in the widest spots was divided into strips, separated by shear zones that ran lengthwise down the channel, indicating across-stream variations in down-stream velocity. The surface crust, once formed, was generally relatively stable on each pool, though sometimes comprised large plates that exhibited the foundering often observed at lava lakes (Duffield, 1972). The surface crust was disrupted where the channel narrowed and sped up between the pools. The crust was also disrupted in these narrow places when they were bridged. In that case, the surface crust was observed piling up against each bridge, forming deep folds before being dragged down into the sump that passed beneath the bridge. The lava surface at the head of the next pool was not crusted when it emerged from beneath the bridge, though a crust formed quickly after the stream was exposed to the air.

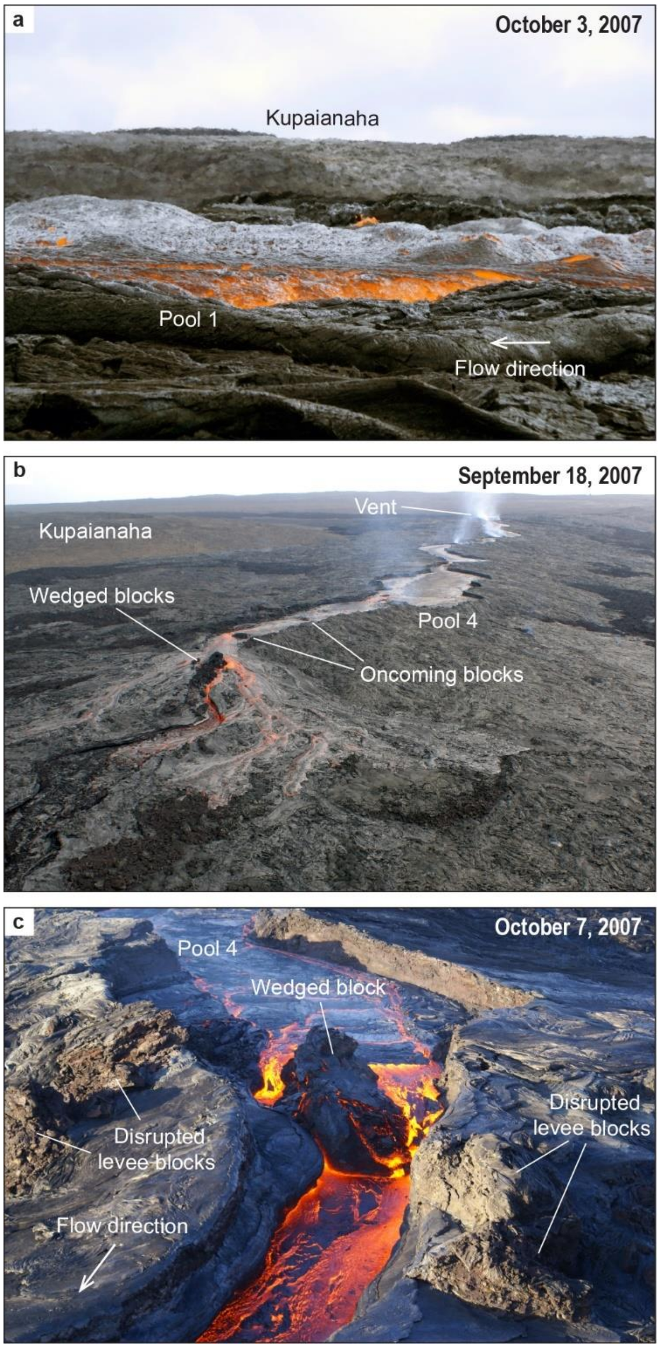

Figure 9. (a) Silvery surface of pool 1 near discharge point hummocky because of gas accumulation in pockets beneath the surface crust, forming domes. Surface of lava stream higher than levee rim (darker gray lava), with height change occurring at shear zone along flow edge where orange, molten lava is exposed. Channel width ~20 m. Photograph by T. Orr, U.S. Geological Survey, October 3, 2007. (b) Large blocks of solidified lava wedged in channel breach and causing overflows. View looking southwest. Photograph by J. Kauahikaua, U.S. Geological Survey, September 18, 2007. (c) Close-up view of large block of solidified lava wedged in channel breach. Channel downstream from block ~15 m wide. Photograph by J. Kauahikaua, U.S. Geological Survey, October 7, 2007.

Patrick et al. (2011) documented the cyclic rise and fall of the lava surface in pool 1 (see Video 24 in Orr, 2011; https://pubs.usgs.gov/ds/621/2007/24_Ep58PerchedChannel_15Nov2007/), which they attributed to ‘gas pistoning’, caused by the generation and collapse of a foam layer beneath the surface crust (e.g., Orr and Rea, 2012; Patrick et al., 2016). The lava surface would gradually rise over a period of minutes during these events, sometimes overflowing the rim, then abruptly fall when the accumulated gas escaped, producing low fountains that traveled with the prevailing current of the lava stream at the shear zones along the edges of the channel.

In one instance during Phase 4, a dome fountain formed abruptly over the discharge point, swelling to a height of ~2 m in less than 5 seconds. The fountain fed a front of lava that advanced over the crusted lava already in the channel, standing a few 10s of cm above it. The dome fountain was steady, inaudible above the background noise of the wind, and lasted for roughly a minute. No associated geophysical signals were recorded on nearby stations. The lava front fed by the low dome fountain migrated down the length of the channel thereafter, overriding the lava channel’s existing crust and causing it to founder. Events that may have been similar were seen several times in imagery captured by a distant time-lapse camera. A more sustained event, also in Phase 4, and lasting ~7 hours, was recorded by a time-lapse camera deployed temporarily near the head of the perched channel. Video 23 in Orr (2011) is a time-lapse movie of this event (https://pubs.usgs.gov/ds/621/2007/23_Ep58FissureDFountain_20Sep2007/).

Failure of the levees was common when the channel was full and would cause the level in the channel to drop several meters as the lava stream escaped through the breach and fed new ‘a‘ā flows that buried those emplaced earlier. Over the course of a day or so, the broken levee would be repaired as massive blocks of solidified lava wedged in the breach, and the channel would fill to overflowing again (Figs. 9b, 9c). In some cases, overflows at the end of the channel may have eroded a notch in the levee, though this was not definitively observed. In most cases, images from a distant webcam suggest that the levee at the end of the channel failed more catastrophically. Either way, impounded lava was released, and the lava level dropped below the channel rim. When the level was low, stationary features appeared within the lava stream. These could have been the tops of large blocks resting on the channel floor, or perhaps the channel floor contained other irregularities. When the lava level came back up, these features became submerged again.

Sections of levee were commonly affected by the formation of generally slow-moving, microlite-rich flows, which we identify as “seeps” (Patrick and Orr, 2012), that oozed from horizontal fractures beneath uplifted sections of the channel levees (Fig. 10a). The seeps were generally composed of dense, dull black to rust-colored, microlite-rich, spiny lava or slabby pāhoehoe, though surface textures more akin to both typical pāhoehoe and ‘a‘ā were also observed. The mean vesicularity is 0.17 (range 0.07–0.32; Fig. 7). In one instance, a section of the perched channel levee was observed to raft a short distance, leaving a scarp that revealed that the levee interior had contained partially molten material at the time of rafting (Figs. 10b, 10c, 10d). Seeps were observed near the levee base in that location both before and after the partial collapse. During Phase 7, a compound pāhoehoe seep with broad uplift scarps, probably fed from pools 2 and 3 and possibly the lower end of pool 1, formed on the southeast side of the channel. Two seeps on the northwest side of pool 3 were also briefly active during this period, and all lava traveling through the perched channel at that time exited through these seeps.

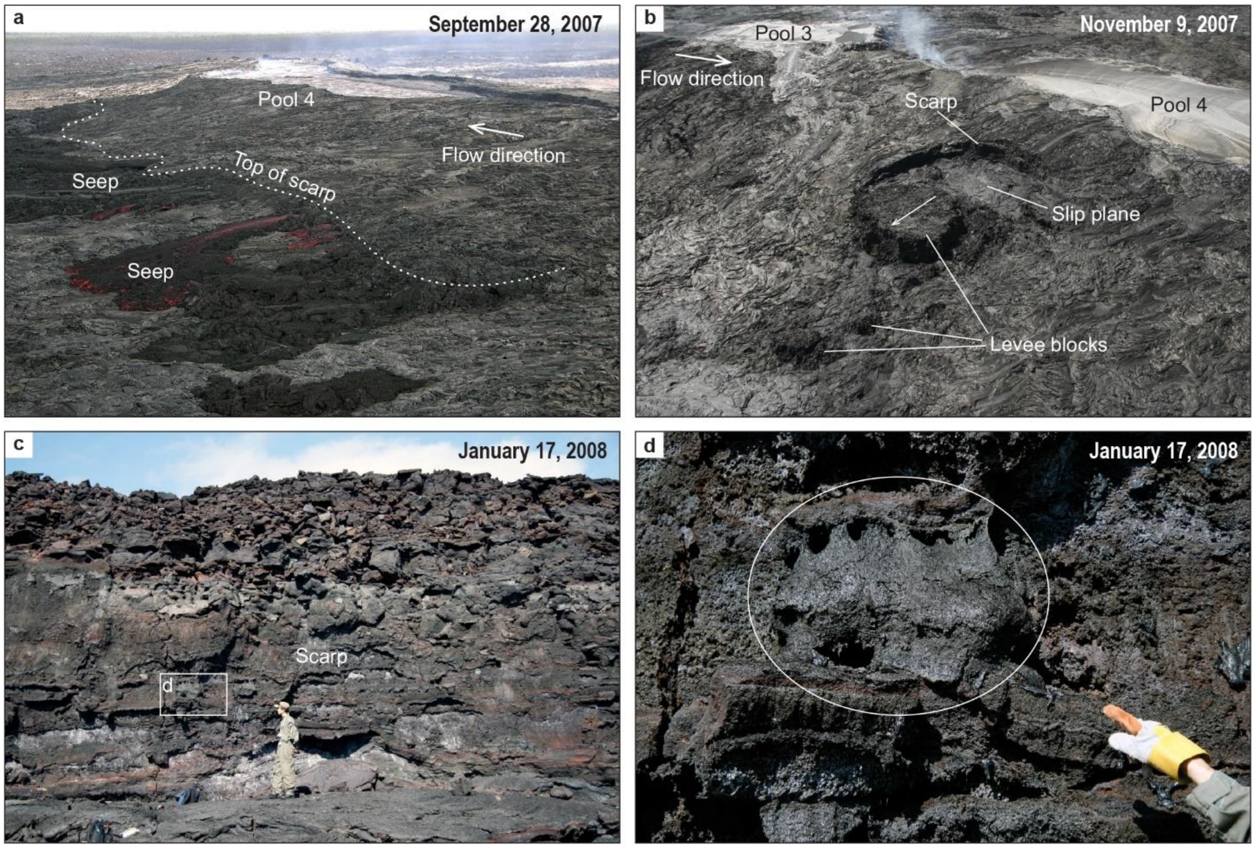

Figure 10. (a) Active and inactive seeps of spiny lava oozing from beneath base of uplifted north flank of perched channel. Dotted white line delineates top of uplift scarp. Photograph by M. Poland, U.S. Geological Survey, September 28, 2007. (b) View of south flank of perched channel at pool 4 showing partial levee collapse. Rafting of levee fragments bracketed by observations on October 31 and November 2, 2007. Arrow on block shows rafting direction. Photograph by T. Orr, U.S. Geological Survey, November 9, 2007. (c) View of scarp formed by partial levee collapse. Slickensides on scarp illustrate hot, partially molten condition of levee at time of partial collapse, as does (d) solidified ooze-out (circled) from cavity on scarp. White box in c shows location of d. Photographs by T. Orr, U.S. Geological Survey, January 17, 2008.

Interpretations of field observations

4.1 Controls on flow length

The series of four flows that initially constructed the channel during late Phase 1 to early Phase 3 (Section 3.2)—the “July 26”, “August 12”, “August 21”, and “August 26” flows—showed both volume-limited and cooling-limited behavior (e.g., Walker et al., 1973; Malin, 1980; Pinkerton and Wilson, 1994; Harris and Rowland, 2009). These flows were fed by breakouts from the perched lava pool that formed over fissure D or from the upper reaches of the incipient perched channel. They were active for between 5 and 17 days, achieved final lengths of between 3.6 km and 6.3 km (measured from the vent along the axis of each flow), and initiated as relatively fast-moving ‘a‘ā. The July 26 and August 12 ‘a‘ā lobes were replaced by spiny lava and slabby pāhoehoe towards the end of their period of activity.

The “August 21” and “August 26” flows had relatively simple emplacement histories, limited by supply of lava. Supply to the “August 21” flow was cut off as lava began to accumulate and overflow the channel near where the flow lobe was diverted. The reduction in supply caused the flow front to stall around 5.2 km from the vent. Supply to the “August 26” flow was cut-off as the channel became progressively blocked at the point where the lava feeding the flow exited the breach in the channel, again causing the flow front to stall, this time about 3.6 km from the vent. Both these flows thus showed volume-limited behavior, as did several smaller, unnamed flows that formed when the levee at the end of the channel failed during subsequent periods when the channel was brimful, and then stalled when the breach became plugged.

The “July 26” and “August 12” flows showed more complicated emplacement history. The “July 26” flow was fed from a breach in the perched lava pool that formed over fissure D and traveled about 3.5 km from its breakout point before its clinkery ‘a‘ā front stalled, despite continued discharge from the fissure D vents. We therefore infer that this branch of the ‘a‘ā flow had reached its cooling-limited length. The flow branch continued to advance, however, with a flow behavior more akin to tube-fed pāhoehoe flows (Fig. 4c), which we infer insulated the lava, removing the cooling limit that determined the run-out length of the parent ‘a‘ā flow. Over time, the input of material from the proximal lava channel appeared to outpace the distal flow’s ability to advance and broaden, and we infer that this caused lava to back up in the channel, leading to new overflows. This, in turn, caused the channelized flow to be redirected into a new flow lobe (the “August 12” flow) at the point where the channel transitioned into dispersed flow, probably by bulldozing the channel levee. This redirection severed supply to the “July 26” flow branch, which stalled at a final length of 5.9 km.

The “August 12” flow behaved in a similar way—it advanced rapidly as a clinkery ‘a‘ā flow at first but slowed as it approached its cooling-limited length and began to produce spiny lava and slabby pāhoehoe. It stalled 6.3 km from the vent when its supply was cut off by a blockage in the channel. Both the “July 26” and “August 12” flows, therefore, showed behavior that was initially cooling-limited, then supply-limited.

4.2 Processes regulating morphology of perched lava channel

Five main processes regulated the evolution of the morphology of the perched lava channel: (1) lava supply; (2) constructional over-plating of the channel levees; (3) levee breaches; (4) channel blockages; and (5) the development of seeps. These processes were related via complex feedbacks. The balance between input (supply) and outflow (breaches, blockages, and seeps) determined the level of lava in the channel. Whenever channel input exceeded outflow, the channel filled to the brim and overflowed, building the levee vertically through constructional overplating. Periods of high lava stand were associated with seeps and levee failure, whereas periods of low lava stand were associated with foundering of the channel rim and bridges, which created blocks that blocked breaches.

The foremost control on lava level was the restriction of outflow from the distal end of the channel—indeed this was instrumental in the formation of the perched channel. The initial evolution of the “July 26” flow branch from a simple channelized flow to a perched channel began with overflows from the channel that over-plated the flow’s ‘a‘ā levees with pāhoehoe. This was caused by the backing up of lava in the channel, as the distal ‘a‘ā flow that the channel was supplying slowed and stopped. Not all lava arriving at the transition between the stable channel and the distal ‘a‘ā flow was able to travel through the incipient tube system within the ‘a‘ā flow to the flow front, where slow-moving spiny lava and slabby pāhoehoe continued to advance. In other words, the distal ‘a‘ā flow acted in part like a dam, and lava flooded the channel levee as a result. Later, once the perched channel was established, periods of levee growth were associated with restriction or blockage of the outflow from pool 4 (Fig. 3, Table 1); periods of lower lava level, throughout the perched channel, were associated with unrestricted outflow from pool 4, sometimes caused by failure of its levees.

Levee failure increased the rate at which lava flowed out of the channel, causing the level in the channel to drop and halting constructional overplating of the levees. Different processes subsequently caused the breach to heal. In some cases, accumulation of lava on the distal flow field may have started a feedback process that caused lava to back up in the channel again and shifted the system back to levee construction. More often though, the breach at the end of the channel was plugged by large blocks. These blocks may have been chunks of material that collapsed from the channel bank or from bridges upstream when the lava level was low (e.g., Harris et al., 2009), agglomerations of foundered surface crust, or possibly a composite of both. This could not be ascertained by the few observations of blocks up close. In those instances, the blocks were draped with rafted crust from the surface of the lava stream that hid their internal makeup.

Variations in supply to the channel were also important in controlling lava level at times. During phase 6, the formation of the TEB flow diverted supply away from the perched channel. Subsequently, during phases 6, 7, and 8, the lava level in the perched channel was controlled by the degree of hydraulic connection between the TEB vent and the perched channel; once this connection was fully severed, the channel was abandoned. Cycles of deflation and inflation (DI events) at Kīlauea’s summit (Anderson et al., 2015) almost certainly affected lava supply to the perched channel. Observations both before (Cervelli and Miklius, 2003) and after (Orr et al., 2015a) episode 58a clearly linked these hours- to days-long summit deformation cycles to variations in discharge on the flow field occurring hours later. More specifically, the deflation phase of these cycles corresponded with a decline in discharge, and discharge increased again during the inflation phase. Identifying discharge changes in the perched channel related to DI events was difficult, however. Aerial observations of the perched channel were usually too infrequent to identify obvious relations, and webcam and time-lapse camera views were of too low resolution, or lacked the necessary perspective, and were often obscured by clouds and rain. In addition, lava level changes caused by competing processes, such as those described above, made unambiguous identification of level changes imparted by DI events impossible. Thus, though we think it likely that DI events caused variations in discharge, this cannot be corroborated by our observations.

Lava seeps and levee failures were observed only when the lava level was high, suggesting a common cause: presumably both were related to increased lava head pressure at the base of the channel during lava high stands. Constructional overplating that increased the levee height likely exacerbated this effect over time. It is likely that seeps played a direct role in facilitating levee failure, by creating a basal slip plane on top of which a section of the levee could slide (Fig. 10b). Rapid vertical growth rates of the levees (Fig. 3) allowed little time for the individual shelly pāhoehoe overflows to cool completely before being buried by subsequent lava, and the levees remained partly molten (Fig. 10d), which may have made it easier for seeps to intrude through the levees without solidifying. Some long-lived seeps fed small channelized ‘a‘ā flows or slabby pāhoehoe. We wonder if, in these cases, the more outgassed lava at the base of the channel had been at least partially swept clear, allowing fresher material to erupt. Our observations were too sparse to determine this.

The occurrence of seeps could be diagnostic of levee instability. Recognition of this correlation was crystallized by the collapse of perched pool levees during episode 58b in 2008 (Patrick and Orr, 2012) and was later used to assess the stability of other perched features that developed at Kīlauea, such as the perched lava channel that formed during Kīlauea's lower ERZ eruption in 2018 (Patrick et al., 2019). Seeps, first described in detail by Peterson and Tilling (1980), are relatively common at Kīlauea, playing an important role in the evolution of many vent structures, such as the 1986–1992 Kupaianaha shield formed during the Puʻuʻōʻō eruption (Orr et al., 2018), the ʻAlae shield formed during the 1969–1974 Mauna Ulu eruption (Peterson and Tilling, 1980), and the 1919–1920 Maunaiki shield (Rowland and Munro, 1993). Indeed, once we began looking, we found seeps on many of the older lava shields and levee structures on Kīlauea. Similar features have subsequently been identified outside Hawaiʻi, such as at the Chaine des Puys volcanic field in France (Saubin, 2014). We also identified a few other instances of levee failures that, in hindsight, were probably associated with seeps. These include a failed levee and flow from an area of ponded lava on the west flank of the Maunaiki shield and a flow from the south flank of a perched lava pool on the west flank of Maunaulu. Like seeps, levee collapses have also been identified at the Chaine des Puys volcanic field (Saubin, 2014), showing that this process is not restricted to Kīlauea.

4.3 Formation and persistence of perched lava channel

To our knowledge, a feature such as the perched channel has not been described before, although perched lava pools and slightly elevated lava channels have both been described independently (e.g., Wilson and Parfitt, 1993; Harris et al., 2009). Moreover, it is unusual for lava flows at Kīlauea to persist in open channelized form for more than a few days, without crusting over to form a tube flow. We propose that there were several factors that conspired together to produce and sustain this unusual phenomenon.

First, the local topography around the channel was somewhat unusual for a proximal flow field at Puʻuʻōʻō. The fissures opened across a broad saddle between Puʻuʻōʻō and Kupaianaha, from which episode 58a lava exited towards the northeast, around the upslope side of Kupaianaha (Fig. 2). The lava was then confined within a very broad trough, around 2 km long, with a very gently sloping thalweg (1–2°). This local topography may have favored dynamic ponding, particularly once the initial ʻaʻā flow had partly dammed the flow path. This ponding and damming caused progressive development of overflow levees that buried the initial channel levees (as in Sparks et al., 1976). Once established, the slope of the lava channel was even lower, at ~0.5°, enhancing this effect. The broad trough and repeated overflows led to the development of a channel that was both wide and deep.

Second, the breadth of the channel is likely to have hindered the formation of a persistent crust. Persistent channel crusts form through accretion of lava to the channel rim, as observed at Mt. Etna (Sparks et al., 1976; Bailey et al., 2006). While the narrower sections of the perched channel bridged over during periods of lava high stand, forming persistent sumps between lava pools, crust was not able to span the broader pools. It is likely that the repeated changes in lava level also hindered crust construction, with removal of support during periods of lava low stand causing marginal crust to founder. The collapse of the bridges between pools during prolonged lava low stands during phase 4 supports this hypothesis. The ready supply of foundered marginal crust may, in turn, have contributed to the self-repair of levee breaches.

Finally, channel persistence also requires that the channel is not abandoned for an extended period. Episodic levee collapse and temporary blockage of the channel did cause parts of the channel to be permanently abandoned—for instance the distal part of the "August 12" branch was abandoned when a blockage formed at the onset of phase 3. But in other instances, parts of the channel were abandoned and then re-occupied later. The formation of the TEB vent caused the perched channel to partly drain several times during phases 6–8, but on each occasion, much of the channel was re-occupied, until the channel was finally abandoned. Re-occupation was likely favored by the breadth and depth of the channel, which presumably mitigated the effects of cooling-induced constriction during re-occupation, as well as by the confining nature of the surrounding topography.

4.4 Discharge rate and local volume flux measurements

Discharge rate is one of the fundamental parameters controlling flow behavior but is commonly difficult to determine. We estimate a time-averaged discharge rate of 3–9 m^3/s for the entirety of episode 58a, based on estimates of the change in total flow field volume over time, and on magmatic gas flux.

The area of the "July 26" flow branch increased by 0.61 km^2 over the ~127-hour interval between mapping missions on July 26 and August 1. Contemporaneous aerial and ground observations found that the edge of the flow was generally 3–6 m thick, and we consider this range to place reasonable bounds on flow thickness. These values give a volume increase that ranges from ~1.8×10^6 m to ~3.7×10^6 m^3 and a dense-rock-equivalent (DRE) discharge rate of 3–6 m^3/s. This is a minimum discharge rate for this period of the eruption, however, because not all lava being erupted was discharging into the "July 26" flow branch—fissures B and C were also active during this period, though their output was much lower than that from fissure D.

Activity at fissures B and C ended before the "August 12" flow branch started, and the "August 12" flow branch captured the lava that had been supplying the more distal part of the "July 26" flow branch. Thus, the eruption's entire output fed the "August 12" flow branch. Based on mapping, the area of the "August 12" branch increased by 0.49 km^2 over the ~72-hour period between August 13 and August 17, giving a volume increase of ~1.5×10^6 m^3 to 3.0×10^6 m^3, again assuming a 3–6-m flow thickness. This equates to a DRE discharge rate of 4–9 m^3/s.

By differencing the flow field DTM (created from foot traverses of the flow field) and the pre-July eruption surface (from airborne InSAR data collected in 2005), a bulk volume of 56.8×10^6 m^3 was found to have been emplaced from July 21 to October 16—a span of 87 days. This corresponds to a DRE discharge rate of ~6 m^3/s, which falls within the range of rates calculated above from differences in flow field area based on mapping. Uncertainty on this estimate of flow volume is much smaller than those based on mapped flow area and estimated thickness. The dominant uncertainty in this case is probably the void space correction, and the uncertainty on the DRE discharge rate is likely ±1 m^3/s.

Gas emission rates at Pu‘u‘ō‘ō have long been known to correlate with discharge rate and are used as a discharge rate proxy (Sutton et al., 2003). From this technique, ~0.08 km^3 of lava was erupted during the interval from the onset of episode 58 through December 2007 (duration 157 days). This equates to a DRE discharge rate of ~6±2 m^3/s (A.J. Sutton, unpublished data; reported in Patrick and Orr, 2012), closely matching the estimates presented above. Moreover, late 2007 coincided with the tail end of a period of increased magma supply to Kīlauea volcano that likewise corresponds to an East Rift Zone discharge rate of 6–7 m^3/s (Poland et al., 2012).

Local volume flux was estimated from direct measurements of channel parameters. The rebar-drop measurement (Section 3.4) indicated a channel depth of ~2 m in the lower channel below pool 4, where the channel was 17 m wide, corresponding to a cross-sectional area of 34 m^2, assuming a rectangular cross section. The surface velocity at that location was 1.1 m/s based on transit times, which corresponds to a mean velocity of 0.7 m/s after accounting for horizontal and vertical velocity variations (Harris et al., 2007). The bulk volume flux thus equals ~24 m^3/s. To estimate DRE volume flux, we assume vesicularity lies in the range 0.49–0.79, which encompasses all values of vesicularity we measured from channel overflows. This gives a DRE volume flux in the range 5–12 m^3/s, which is consistent with the values we calculated above.

At pool 2, ~500 m downstream from the vent, where the channel was ~20 m wide, the depth of the channel was estimated to be between 8 and 18 m, bounded by the rebar-drop measurement and consideration of levee height above the pre-existing ground surface (Section 3.4). These give a minimum cross-sectional area of 160 m^2 and a maximum cross-sectional area of 360 m^2. The surface velocity at that location was measured at 0.5 m/s from transit time, which corresponds to a mean velocity of 0.3 m/s. The bulk volume flux thus lies in the range 48–108 m^3/s. Using the same vesicularity bounds as before (0.49–0.79), this gives DRE volume flux in the range 10–55 m^3/s, which is higher than the time-averaged discharge rates calculated above with different techniques.

Using a similar approach, the average surface velocity of pool 1 during November 15–17, based on webcam imagery, was 0.18 m/s, which corresponds to a mean velocity of 0.12 m/s. The width of the channel where the velocity was measured was ~45 m, and it was at least 10 m deep, based on the estimated drop in lava level at the onset of the TEB flow. This equates to a rectangular cross-sectional area of ~450 m^2. The maximum depth based on levee height was ~30 m (Fig. 5), which corresponds to a cross-sectional area of ~1,350 m^2. The bulk volume flux thus lies in the range 54–162 m^3/s. Using the same vesicularity bounds as before, this gives DRE volume flux in the range 11–83 m^3/s, which is close to the discharge rate calculated previously for pool 2.

There are two potential explanations for the discrepancy between the volume fluxes estimated for pools 1 and 2, and the much lower estimates for the time-averaged discharge rate and volume flux in the lower channel: (1) the measurements in pools 1 and 2 were collected during periods of unusually high discharge rate; or (2) the assumptions underpinning one set of measurements are violated. The first explanation is unlikely, because there was no other evidence of elevated discharge rates in early October (pool 2 and lower channel measurements) or mid-November (pool 1 measurements). It is not feasible that a ~10-fold increase in discharge rate could have been sustained over the 2-day window of measurements of the velocity of pool 1 without additional corroborating field evidence, such as extensive overflows from the channel. Furthermore, the snapshot estimates for pool 2 and the lower channel were made on the same day yet yield very different volume fluxes. The second explanation therefore appears much more likely.

The uncertainties on the estimates of gas output and change in flow field volume are sufficiently well constrained that we are confident that the true time-averaged discharge rate lies within the range 3–9 m^3/s, based on several independent estimates. By contrast, the estimates of the volume flux in the pools and channel are predicated on the unverified (and unverifiable) assumption that the vertical velocity profile within the flowing lava matches the parabolic profile inferred by Harris et al. (2007). This profile is based, in turn, upon the assumption of Newtonian rheology and homogeneous viscosity. There are several lines of evidence that point to violation of these assumptions in pools 1 and 2.

5. Synthesis and Implications

In this section, we synthesize the field observations presented and discussed in Sections 3 and 4, to construct a conceptual model for the formation, structure, and behavior of the perched channel system. The model, whilst somewhat speculative, sets these observations within a physical framework that sheds light on a range of fundamental processes that may also operate in other settings.

5.1 Vertical structure of the lava in the channel

There are several lines of evidence that strongly imply that the lava in the perched channel had a vertical vesicularity gradient, with foamy lava at the surface overlying denser lava. Most obviously, overflows produced highly vesicular shelly pāhoehoe, whereas seeps, which are interpreted to sample lava from deeper in the channel, typically produced dense spiny lava and slabby pāhoehoe. Gas pistoning activity and the observation of lava standing slightly higher than the channel rim (Fig. 9a) also imply very high vesicularity in the upper meters of the channelized flow. Three physical processes inevitably require that the vesicularity decreases downwards. First, the buoyant ascent of bubbles will tend to decrease vesicularity at depth and increase vesicularity at shallower levels. Second, drainage of melt in the films between bubbles in the shallow foam will tend to increase its vesicularity. Finally, increasing hydrostatic pressure with depth will tend to decrease gas volume both through equation-of-state response of bubbles, and through increased volatile solubility (See Appendix). Figure 11 shows the vertical vesicularity profile that we compute, using the method presented in the Appendix, for lava in pools 1, 3, and 4. The most notable feature of these profiles is that accounting for the pressure-dependent solubility of H_2O leads to a sharp transition from a foamy surface layer to a fully dense lower layer at a depth of only a few meters.

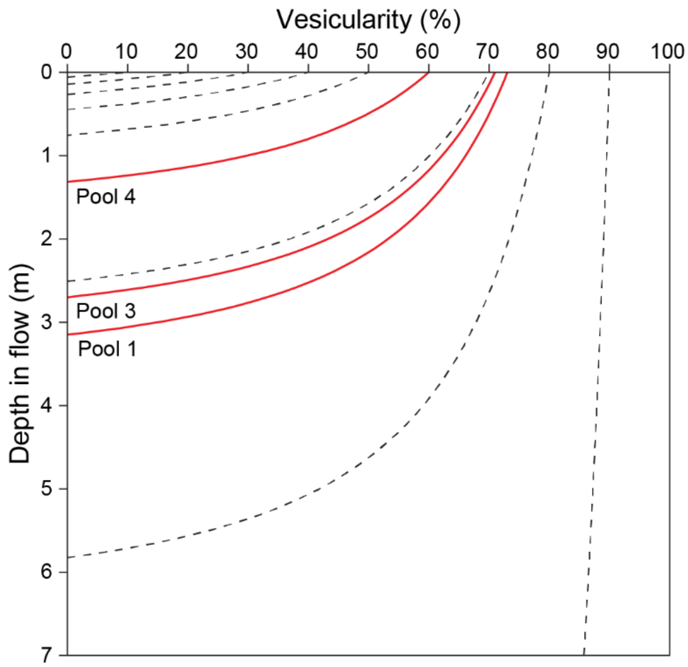

Figure 11. Computed vesicularity profiles for pools 1, 3, and 4 (red lines). Vesicularity of surface lava in each pool estimated from measurements of clasts (Fig. 10): 73%, 71%, and 60% respectively in pools 1, 3, and 4. Profile calculated following approach presented in Appendix, which accounts for increasing gas density and solubility with increasing depth. Dashed black lines show computed solutions for surface vesicularity at 10% intervals. Note that upper vesicular layer transitions sharply into fully dense lava at depth of only a few meters.

Gas that accumulated in the shallow foam was released over time, via bursting or disruption of bubbles, which was observed, and probably also via percolation and diffusion through the upper crust. This gas release was particularly evident during gas pistoning events, and in the shear zones at channel margins. Consequently, the vertical vesicularity distribution of the shallow foam likely had a complex evolution as the lava was transported down the channel.

The presence of a strong vertical variation in vesicularity in the flow has several important implications for flow structure, which ultimately explain various observed phenomena. Perhaps most importantly for transport processes, the rheology of lava depends on its vesicularity, so the presence of a vertical vesicularity variation also implies a vertical rheology variation. This rheology variation, in turn, implies complex vertical velocity variation. It is beyond the scope of this work to analyze the velocity structure in detail, but observations of the flow behavior allow some qualitative interpretations.

The behavior of the lava boats that were observed within the channel yields insight into the velocity and vesicularity structure. The lava boats are thought to have been composed of foundered channel rim and agglomerations of lava crust accumulated during transport, and presumably had a mean density somewhere between that of the foamy lava, and the underlying dense lava. Consequently, the boats would have floated at a depth such that their center of mass lay within the zone of transition from foamy to dense lava, and oriented, for stability, such that their least dimension was aligned vertically (assuming homogeneous density). Some larger boats had dimensions around 3–5 m in map view, suggesting that their vertical dimension was <3 m; hence, for a boat of this size to be observed at the surface, the thickness of the foam layer must have been less than roughly half of the vertical dimension, suggesting a foam layer thickness of ~1 m. Boats were observed only in the distal end of pool 4, and progressive outgassing during transport likely thinned the foam layer by the time lava reached there, hence 1 m might be viewed as a minimum foam layer thickness. The boats traveled much more slowly (meters per hour) than the surface of the lava flow (decimeters per second). The boats' velocity must have reflected some integrated mean of the lava flow velocity over their vertical extent; hence, their relatively slow velocity indicates that their keels were embedded in very slow-moving or stagnant lava, implying a strong velocity gradient of the top few meters of the lava flow.

The rheology of magmatic foams (vesicularity >0.64) is still poorly characterized, but foams in general are known to have an appreciable yield stress (Princen and Kiss, 1989). The effective viscosity of bubbly magma (vesicularity <64%) is known to depend on vesicularity and strain rate, via the capillary number $\mathrm{Ca} = \mu a \dot{\gamma} / \Gamma$, where μ is the melt viscosity, a is the bubble radius, $\dot{\gamma}$ is the strain rate, and Γ is the surface tension: vesicles act to increase viscosity for $\mathrm{Ca} < 1$, and decrease viscosity for $\mathrm{Ca} > 1$ (Mader et al, 2013). On this basis, we propose that the foamy upper layer of the lava 'slides' as a coherent (but deformable) body, over the dense underlying lava, lubricated by a layer of bubbly magma that is in the high capillary number regime. We can make a crude estimate of feasibility by assuming that the velocity difference between the surface foam and underlying dense lava (of order 0.5 m/s) is accommodated by a bubbly layer of order 0.1 m thick, giving a characteristic strain rate across the layer of $\dot{\gamma} \approx 5$ s^{-1}. Assuming values of $\mu = 200$ Pa s (using Giordano et al., 2008, for a typical Kīlauea composition and eruption temperature), $0.001 \lesssim a \lesssim 0.01$ m (based on our observations of vesicular crust), and $\Gamma = 0.2$ N/m (Khitarov et al., 1979; Colucci et al., 2016), gives $5 \lesssim \mathrm{Ca} \lesssim 50$, which implies that bubbles would indeed act to decrease the viscosity of the lava, creating a lubricating layer.

Decoupling of surface lava motion from the motion of underlying dense lava also explains the high volume-flux estimates for pools 1 and 2. For example, the mean surface crust vesicularity of 0.73 measured for pool 1 (Section 3.4) corresponds to a foam layer 3.14 m thick, with an average vesicularity of 0.54. Using the same pool 1 width and surface velocity as before (Section 4.4) gives a DRE flux of 12 m^3/s, which is as much as a factor of 7 smaller than the estimated flux calculated using the velocity profile assumption of Harris et al. (2007) and close to the estimates of time-averaged discharge rate determined by other methods. The fact that the volume flux estimated for the channel below pool 4 does not require correction in this way is consistent with its much shallower depth (~2 m). The dense lava was likely trapped in pool 4 while the foamy lava escaped over the shallow spillway that fed the lower channel. The short distance between the spillway and the measurement location likely precluded the formation of any appreciable lower, slow-moving dense layer.

We summarize our conceptual model for the vertical pressure, vesicularity, rheology, and velocity structure in the channel in Figure 12.

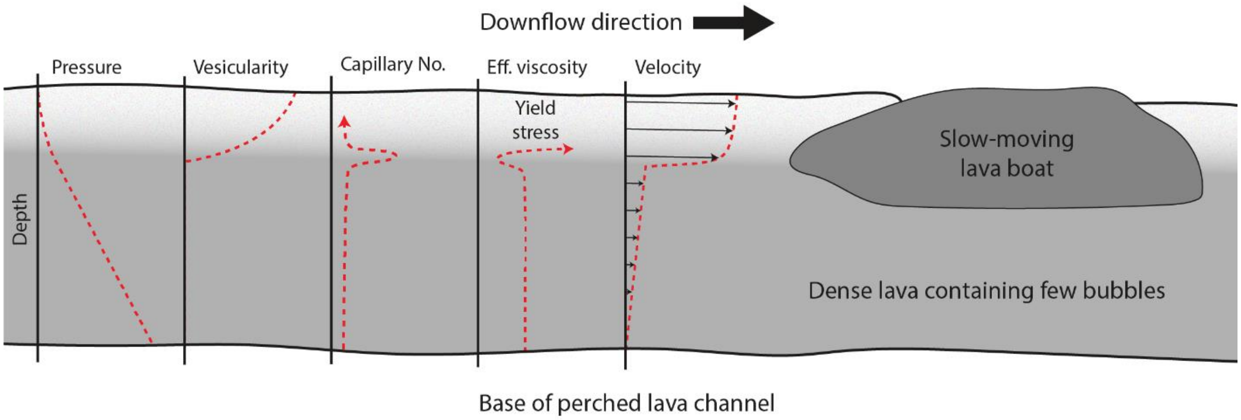

Figure 12. Schematic cartoon showing inferred vertical distribution of pressure, vesicularity, capillary number, effective viscosity, and downstream velocity of lava stream in perched lava channel. Sharp change in vesicularity at depth of a few meters effectively creates two-layer system, with fast-moving layer of foamy lava overlying slow-moving layer of dense lava.

5.2 Seeps and levee failure

The inferred vertical vesicularity structure of the lava is also consistent with, and helps to explain, the behavior of seeps and levee failures. Levees are constructed primarily from overflows of shelly pāhoehoe—perhaps somewhat compacted when growth rates are high enough to retain sufficient heat—intermingled with denser accretions. The typical vesicularity of the levees is therefore relatively high (our measured values ranged from 0.49 to 0.79 for overflow from all four pools), although not as high as the foamy lava at the surface of the channel. The geometry and position of the seeps indicates that they form as lateral ‘sills’ that intrude through the levee pile, perhaps exploiting weaknesses at sub-horizontal surfaces between stacks of overflows formed during periods of levee growth. The seeps also create scarps where they exit the levee, indicating some degree of uplift of the levee.

For lava to intrude into the levee, we expect that the hydrostatic pressure in the lava at the intrusion depth must exceed the lithostatic pressure in the levee pile. For this to occur, the vertically integrated average density of the lava must exceed the average density of the levee pile and, presumably, the greater the excess lava pressure, the greater the likelihood of intrusion. This is supported by the observation that seeps and levee failures are associated with periods of lava high stand. This behavior can occur only if the lava becomes, on average, denser as it deepens—this is consistent with the proposed vertical vesicularity profile in the lava (Figs. 11, 12). The uplift of the levee caused by seeps also suggests that buoyancy may play a role; once lava has begun to intrude, the levee can ‘float’ on the dense lava. This rafting (Fig. 10b) may contribute to levee failure and provides a physical mechanism to explain the observed association between the occurrence of seeps and levee failure.

6. Conclusions

Episode 58a of Kīlauea’s Pu‘u‘ō‘ō eruption was most notable for the formation of a remarkable perched lava channel, active for 4 months, which exhibited characteristics of both a channelized flow and a perched lava pool. We calculate a time-averaged discharge rate in the range 3–9 m^3/s

for this activity. The channel levees grew mainly by repeated overflows and eventually stood as high as 45 m, forming a ridge topped by a series of four elongate and interconnected lava pools. The perched lava channel was gradually abandoned after a new breakout at the vent began feeding lava in a different direction.

The lava channel initially fed clinkery ‘a‘ā flows that stalled upon reaching their cooling-limited length, forming a compound ‘a‘ā flow field, but lava continued to move through the core of the ‘a‘ā flow to its front, and the flow proceeded to advance as spiny lava and slabby pāhoehoe. This latter phase of the flows ended when the supply of lava to the flow front was interrupted. Thus, these early flows exhibited both cooling-limited and volume-limited behaviors, with each aspect associated with a different lava flow texture. Later flow branches were volume limited only. The perched lava channel developed thereafter, creating a compound pāhoehoe flow field (Walker, 1971).

The 2007 activity provided the opportunity to observe closely the development of lava seeps, which are relatively outgassed flows of spiny lava and slabby pāhoehoe that extrude from the flanks of rapidly growing rootless shields and perched lava pools. We also observed and documented the development of the perched lava channel and its levees, which proved to be unstable. In this case, as the perched channel grew vertically, failures of the levee at the end of the channel allowed the channel to partly drain as it fed rapidly moving flows. These flows ended when the breach in the levee became plugged by large blocks transported down the channel. We infer that levee failures may have been enabled by the formation of seeps, which burrowed beneath and uplifted the channel levees, forming scarps along which the dense lava erupted. The occurrence of seeps, therefore, is diagnostic of levee instability.

Based on a number of lines of evidence, including (1) the contrasting textures of the overflow and seep flows (highly vesicular shelly pāhoehoe and dense spiny lava, respectively), (2) consideration of bulk discharge rate and local volume flux in the channel, and (3) the motion of ‘lava boats’, we infer that the lava in the channel had a strong vertical vesicularity variation. The uppermost lava was a layer of highly vesicular foam (porosity up to 0.79), perhaps 1–3 m thick, which overlaid a much thicker layer of dense lava. The strong vertical stratification in vesicularity led, in turn, to vertical variation in rheology and flow velocity of the lava. This stratification is likely to be a feature of any sufficiently deep lava flow, with far-reaching implications for its rheology, velocity, and emplacement behavior.

CRediT authorship contribution statement

Tim R. Orr: Conceptualization, Investigation, Writing - original draft, Writing - review & editing, Visualization, Supervision, Project administration. Matt R. Patrick: Conceptualization, Investigation, Writing - original draft, Writing - review & editing. Edward W. Llewellin: Conceptualization, Writing - original draft, Writing - review & editing, Visualization.

Declaration of competing interest

The authors declare that they have no known competing financial interests or personal relationships that could have appeared to influence the work reported in this paper.

Acknowledgements

Eruption response is a team effort, and we are grateful to the staff and volunteers of the Hawaiian Volcano Observatory who helped collect the robust observations that contributed to a better understanding of eruptive activity during 2007–2008. We especially thank Dave Sherrod (USGS Cascades Volcano Observatory) and Arkin Tapia (Universidad de Panamá) for the herculean and exceedingly treacherous task of collecting topographic data for an actively developing flow field via foot traverse with backpack mounted kinematic GPS receivers; Liliana DeSmither for assistance calculating lava porosity; and David Okita for his expert piloting, which has facilitated unparalleled access to eruptive activity at Kīlauea for several decades. EWL acknowledges funding from the Royal Society via International Exchanges Grant IE130961. Natalia Deligne, Scott Rowland, and an anonymous reviewer provided helpful reviews that greatly improved the manuscript. Any use of trade, firm, or product names is for descriptive purposes only and does not imply endorsement by the U.S. Government.

References Cited

Anderson K., Poland M., Johnson J., and Miklius A., 2015, Episodic deflation-inflation events at Kīlauea Volcano and implications for the shallow magma system. In: Carey, R., Poland, M., Cayol, V., and Weis, D. (eds), Hawaiian Volcanism: From Source to Surface. Wiley, Hoboken, New Jersey, p. 229–250. [https://doi.org/10.1002/9781118872079.ch11]

Bailey, J.E., Harris, A.J.L., Dehn, J., Calvari, S., and Rowland, S.K., 2006, The changing morphology of an open lava channel on Mt. Etna. Bulletin of Volcanology, 68(6), p. 497–515. [https://doi.org/10.1007/s00445-005-0025-6]

Calvari, S., Neri, M., Pinkerton, H., 2003, Effusion rate estimations during the 1999 summit eruption on Mount Etna, and growth of two distinct lava flow fields. Journal of Volcanology and Geothermal Research, 119(1), p. 107–123. [https://doi.org/10.1016/S0377-0273(02)00308-6]

Cervelli, P.F., and Miklius, A., 2003, The shallow magmatic system of Kilauea volcano. In: Heliker, C., Swanson, D.A., and Takahashi, T.J. (eds), The Puʻu ʻŌʻō-Kupaianaha Eruption of Kilauea Volcano, Hawaii—The First 20 Years. U.S. Geological Survey Professional Paper 1676, p. 149–163. [https://doi.org/10.3133/pp1676]

Colucci, S., Battaglia, M. and Trigila, R., 2016, A thermodynamical model for the surface tension of silicate melts in contact with H2O gas. Geochimica et Cosmochimica Acta, 175, p.113–127. [https://doi.org/10.1016/j.gca.2015.10.037]

Duffield, W.A., 1972, A naturally occurring model of global plate tectonics. Journal of Geophysical Research, 77(14), p. 2543–2555. [https://doi.org/10.1029/JB077i014p02543]

Giordano, D., Russell, J.K. and Dingwell, D.B., 2008, Viscosity of magmatic liquids: a model. Earth and Planetary Science Letters, 271(1-4), p. 123–134. [https://doi.org/10.1016/j.epsl.2008.03.038]

Harris, A., and Rowland, S., 2009, Effusion rate controls on lava flow length and the role of heat loss: a review. Studies in volcanology: the legacy of George Walker. Special Publications of IAVCEI, 2, p. 33–51.

Harris, A., Dehn, J., and Calvari, S., 2007, Lava effusion rate definition and measurement: a review. Bulletin of Volcanology, 70(1), p. 1–22. [https://doi.org/10.1007/s00445-007-0120-y]

Harris, A.J.L., Favalli, M., Mazzarini, F., and Hamilton, C.W., 2009, Construction dynamics of a lava channel. Bulletin of Volcanology, 71(4), p. 459–474. [https://doi.org/10.1007/s00445-008-0238-6]

Harris, A.J.L., Rowland, S.K., Villeneuve, N., and Thordarson, T., 2016, Pāhoehoe, ʻaʻā, and block lava: an illustrated history of the nomenclature. Bulletin of Volcanology, 79(7), p. 1–34. [https://doi.org/10.1007/s00445-016-1075-7]

Heliker, C., and Mattox, T.N., 2003, The first two decades of the Puʻu ʻŌʻō-Kūpaianaha eruption; chronology and selected bibliography. In: Heliker, C., Swanson, D.A., and Takahashi, T.J. (eds), The Puʻu ʻŌʻō-Kupaianaha Eruption of Kilauea Volcano, Hawaii—The First 20 Years. U.S. Geological Survey Professional Paper 1676, p. 1–27. [https://doi.org/10.3133/pp1676]

Heliker, C., Kauahikaua, J., Sherrod, D.R., Lisowski, M., and Cervelli, P., 2003, The rise and fall of Puʻu ʻŌʻō cone, 1983–2002. In: Heliker, C., Swanson, D.A., and Takahashi, T.J. (eds), The Puʻu ʻŌʻō-Kupaianaha Eruption of Kilauea Volcano, Hawaii—The First 20 Years. U.S. Geological Survey Professional Paper 1676, p. 29–51. [https://doi.org/10.3133/pp1676]

Houghton, B.F., and Wilson, C.J.N., 1989, A vesicularity index for pyroclastic deposits: Bulletin of Volcanology, 51(6), p. 451–462.[https://doi.org/10.1007/BF01078811]

Khitarov, N.I., Lebedev, E.B., Dorfman, A.M., and Bagdasarov, N.S., 1979, Effect of temperature, pressure and volatiles on the surface tension of molten basalt. Geochemistry International, 16(5), 78–86.

Lesher, C.E. and Spera, F.J., 2015, Thermodynamic and transport properties of silicate melts and magma. In: Sigurdsson, H., Houghton, B., Rymer, H., Stix, J., and McNutt, S., editors, The Encyclopedia of Volcanoes (Second Edition), Elsevier, p. 113–141. [https://doi.org/10.1016/B978-0-12-385938-9.00005-5]

Lipman, P.W., and Banks, N.G., 1987, Aa flow dynamics, Mauna Loa 1984. In: Decker, R.W., Wright, T.L., and Stauffer, P.H. (eds), Volcanism in Hawaii. U.S. Geological Survey Professional Paper 1350, p. 1527–1567. [https://doi.org/10.3133/pp1350]

Mader, H.M., Llewellin, E.W. and Mueller, S.P., 2013, The rheology of two-phase magmas: A review and analysis. Journal of Volcanology and Geothermal Research, 257, p.135–158. [https://doi.org/10.1016/j.jvolgeores.2013.02.014]

Malin, M.C., 1980, Lengths of Hawaiian lava flows. Geology 8(7), p. 306–308. [https://doi.org/10.1130/0091-7613(1980)8<306:LOHLF>2.0.CO;2]

Neal, C.A., Brantley, S.R., Antolik, L., Babb, J.L., Burgess, M., Calles, K., Cappos, M., Chang, J.C., Conway, S., Desmither, L., Dotray, P., Elias, T., Fukunaga, P., Fuke, S., Johanson, I.A., Kamibayashi, K., Kauahikaua, J., Lee, R.L., Pekalib, S., Miklius, A., Million, W., Moniz, C.J., Nadeau, P.A., Okubo, P., Parcheta, C., Patrick, M.R., Shiro, B., Swanson, D.A., Tollett, W., Trusdell, F., Younger, E.F., Zoeller, M.H., Montgomery-Brown, E.K., Anderson, K.R., Poland, M.P., Ball, J.L., Bard, J., Coombs, M., Dietterich, H.R., Kern, C., Thelen, W.A., Cervelli, P.F., Orr, T., Houghton, B.F., Gansecki, C., Hazlett, R., Lundgren, P., Diefenbach, A.K., Lerner, A.H., Waite, G., Kelly, P., Clor, L., Werner, C., Mulliken, K., Fisher, G., and Damby, D., 2019, The 2018 rift eruption and summit collapse of Kīlauea Volcano: Science, 363(6425), p. 367–374. [https://doi.org/10.1126/science.aav7046]

Orr, T.R., 2011, Selected time-lapse movies of the East Rift Zone eruption of Kīlauea Volcano, 2004–2008, U. S. Geological Survey Data Series 621, 15 p., 26 movies. [https://doi.org/10.3133/ds621]

Orr, T.R., and Rea, J.C., 2012, Time-lapse camera observations of gas piston activity at Puʻu ʻŌʻō, Kīlauea volcano, Hawaiʻi. Bulletin of Volcanology, 74(10), p. 2353–2362. [https://doi.org/10.1007/s00445-012-0667-0]

Orr, T.R., Bleacher, J.E., Patrick, M.R., and Wooten, K.M., 2015a, A sinuous tumulus over an active lava tube at Kīlauea Volcano: Evolution, analogs, and hazard forecasts. Journal of Volcanology and Geothermal Research, 291, p. 35–48. [https://doi.org/10.1016/j.jvolgeores.2014.12.002]

Orr, T.R., Poland, M.P., Patrick, M.R., Thelen, W.A., Sutton, A.J., Elias, T., Thornber, C.R., Parcheta, C., and Wooten, K.M., 2015b, Kīlauea's 5–9 March 2011 Kamoamoa Fissure Eruption and Its Relation to 30+ Years of Activity From Puʻu ʻŌ ʻō. In: Carey, R., Poland, M., Cayol, V., and Weis, D. (eds), Hawaiian Volcanism: From Source to Surface. Wiley, Hoboken, New Jersey, p. 393–420. [https://doi.org/10.1002/9781118872079.ch18]

Orr, T.R., Ulrich, G.E., Heliker, C., DeSmither, L.G., and Hoffmann, J.P., 2018, The Puʻu ʻŌʻō eruption of Kīlauea Volcano, Hawaiʻi—Episode 21 through early episode 48, June 1984–April 1987. U.S. Geological Survey Scientific Investigations Report 2018-5109, 107 p. [https://doi.org/10.3133/sir20185109]

Patrick, M., and Orr, T., 2012, Rootless shield and perched lava pond collapses at Kīlauea Volcano, Hawai'i. Bulletin of Volcanology, 74(1), p. 67–78. [https://doi.org/10.1007/s00445-011-0505-9]

Patrick, M.R., Orr, T., Wilson, D., Dow, D., and Freeman, R., 2011, Cyclic spattering, seismic tremor, and surface fluctuation within a perched lava channel, Kīlauea Volcano. Bulletin of Volcanology, 73(6), p. 639–653. [https://doi.org/10.1007/s00445-010-0431-2]

Patrick, M.R., Orr, T., Sutton, A.J., Lev, E., Thelen, W., and Fee, D., 2016, Shallowly driven fluctuations in lava lake outgassing (gas pistoning), Kīlauea Volcano. Earth and Planetary Science Letters, 433, p. 326–338. [https://doi.org/10.1016/j.epsl.2015.10.052]

Patrick, M.R., Dietterich, H.R., Lyons, J.J., Diefenbach, A.K., Parcheta, C., Anderson, K.R., Namiki, A., Sumita, I., Shiro, B., and Kauahikaua, J.P., 2019, Cyclic lava effusion during the 2018 eruption of Kīlauea Volcano. Science, 366(6470). [https://doi.org/10.1126/science.aay9070]

Patrick, M.R., Orr, T.R., Swanson, D., Houghton, B.F., Wooten, K.M., Desmither, L., Parcheta, C., and Fee, D., 2021, Kīlauea’s 2008–2018 summit lava lake—Chronology and eruption insights. U.S. Geological Survey Professional Paper 1867A, 50 p. [https://doi.org/10.3133/pp1867A]

Peterson, D.W. and Tilling, R.I., 1980, Transition of basaltic lava from pahoehoe to aa, Kilauea Volcano, Hawaii: Field observations and key factors. Journal of Volcanology and Geothermal Research, 7(3), p. 271–293. [https://doi.org/10.1016/0377-0273(80)90033-5]

Pinkerton, H., and Wilson, L., 1994, Factors controlling the lengths of channel-fed lava flows. Bulletin of Volcanology, 56(2), p. 108–120. [https://doi.org/10.1007/bf00304106]

Poland, M.P., Miklius, A., Jeff Sutton, A., and Thornber, C.R., 2012, A mantle-driven surge in magma supply to Kīlauea Volcano during 2003-2007. Nature Geoscience, 5(4), p. 295–300. [https://doi.org/10.1038/ngeo1426]

Princen, H.M. and Kiss, A.D., 1989, Rheology of foams and highly concentrated emulsions: IV. An experimental study of the shear viscosity and yield stress of concentrated emulsions. Journal of Colloid and Interface Science, 128(1), p.176–187. [https://doi.org/10.1016/0021-9797(89)90396-2]

Rowland, S.K., Walker, G.P.L., 1987, Toothpaste lava: Characteristics and origin of a lava structural type transitional between pahoehoe and aa. Bulletin of Volcanology, 49(4), p. 631–641. [https://doi.org/10.1007/bf01079968]

Rowland, S.K., and Munro, D.C., 1993, The 1919–1920 eruption of Mauna Iki, Kilauea: chronology, geologic mapping, and magma transport mechanisms. Bulletin of Volcanology, 55(3), p. 190–203. [https://doi.org/10.1007/bf00301516]

Saubin, E., 2014, Etude dynamique, texturale et rhéologique de laves mises en place sur une pente forte—Exemple de Gravenoire dans la chaîne des Puys. Ph.D. Thesis, Universite Blaise Pascal, Clermont-Ferrand, France. 25 p.

Sparks, R.S.J., Pinkerton, H., and Hulme, G., 1976, Classification and formation of lava levees on Mount Etna, Sicily. Geology 4(5), p. 269–271. [https://doi.org/10.1130/0091-7613(1976)4<269:cafoll>2.0.co;2]

Sutton, A.J., Elias, T., and Kauahikaua, J., 2003, Lava-effusion rates for the Puʻu ʻŌʻō–Kupaianaha eruption derived from SO2 emissions and very low frequency (VLF) measurements, in Heliker, C., Swanson, D.A., and Takahashi, T.J., eds., The Puʻu ʻŌʻō–Kupaianaha eruption of Kīlauea Volcano, Hawaii; the first 20 years. U.S. Geological Survey Professional Paper 1676, p. 137–148.

Walker, G.P.L., 1971, Compound and simple lava flows and flood basalts. Bulletin of Volcanology, 35(3), p. 579–590. [https://doi.org/10.1007/bf02596829]

Walker, G.P.L., Guest, J.E., and Skelhorn, R.R., 1973, Mount Etna and the 1971 eruption - Lengths of lava flows. Philosophical Transactions of the Royal Society of London. Series A, Mathematical and Physical Sciences 274(1238), p. 107–118. [https://doi.org/10.1098/rsta.1973.0030]

Wilson, L., and Parfitt, E.A., 1993, The formation of perched lava ponds on basaltic volcanoes: the influence of flow geometry on cooling-limited lava flow lengths. Journal of Volcanology and Geothermal Research, 56(1), p. 113–123. [http://dx.doi.org/10.1016/0377-0273(93)90053-T]

Wolfe, E.W., Neal, C.A., Banks, N.G., and Duggan, T.J., 1988, Geologic observations and chronology of eruptive events. In: Wolfe, E.W. (ed.), The Puu Oo eruption of Kilauea Volcano, Hawaii; episodes 1 through 20, January 3, 1983, through June 8, 1984: U.S. Geological Survey Professional Paper 1463, p. 1–97. [https://doi.org/10.3133/pp1463]

Appendix. Vesicularity profile in a lava flow

Both the density and solubility of the volatile gases contained in bubbles in lava increase with pressure. Consequently, we expect gas volume fraction to decrease with increasing depth in a lava flow, in response to the increase in hydrostatic pressure. We compute lava vesicularity ϕ as a function of depth z using a simple spreadsheet approach, assuming that H2O is the only volatile species. The spreadsheet is available as an electronic supplement.

The lava column is divided into a stack of N horizontal layers of equal thickness h. The contribution of layer i to the hydrostatic pressure is calculated as

$$\Delta p_i = \rho(1-\phi_i)gh\,, \qquad \text{Eq. A1}$$

where ρ is the melt density and g is gravitational acceleration. Note that a subscript i indicates the value of a quantity for layer i, where where $i = 1, 2, \ldots, N$. The hydrostatic pressure acting on the top of layer i is found by summing the contribution of the overlying layers

$$p_i = \sum_{j=0}^{i-1} \Delta p_j\,, \qquad \text{Eq. A2}$$

where the contribution of atmospheric pressure p_0 is captured by taking $\Delta p_0 = p_0$, such that $p_1 = p_0$. The solubility of H_2O in layer i is calculated following the equation of Iacono-Marziano et. al (2012) using parameter values appropriate for typical Kilauea basalt:

$$C_i = \exp\left(0.54 \ln p_i - 2.56 + 0.02\frac{p_i}{T}\right), \qquad \text{Eq. A3}$$

where C_i is in wt.%, p_i is in bar (i.e., 10^5 Pa), and T is the absolute temperature of the lava in Kelvin. The density ρ_g of gaseous H_2O in layer i is given by the ideal gas law

$$\rho_{g,i} = m_{\mathrm{H2O}}\frac{p_i}{RT}\,, \qquad \text{Eq. A4}$$

where m_{H2O} is the molar mass of H_2O and R is the ideal gas constant.

We assume that the total number of moles of H_2O (the sum of the dissolved and exsolved components) per unit volume of melt, n, is the same in every layer, and that the two components are at equilibrium. The number of moles of dissolved H_2O per unit volume of melt in layer i is given by

$$n_{d,i} = \frac{C_i\rho}{100 m_{\mathrm{H2O}}}\,, \qquad \text{Eq. A5}$$

and the number of moles of exsolved (gaseous) H_2O per unit volume of melt in layer i is given by

$$n_{e,i} = \frac{\rho_{g,i}}{m_{\mathrm{H2O}}}\left(\frac{\phi_i}{1-\phi_i}\right). \qquad \text{Eq. A6}$$

We take as input the vesicularity of the top layer ϕ_1 and the ambient pressure acting on the top layer p_0. From equations A1–A6 we can compute the total number of moles $n = n_{d,i} + n_{e,i} = \mathrm{const}$ and the contribution to the hydrostatic pressure arising from layer 1 (i.e., Δp_1). In every other layer (i.e., for $i > 1$) the number of moles of dissolved H_2O per unit volume of melt is calculated (Eqs. A3 and A5) using the appropriate pressure calculated from Eq. A2, and the number of moles of exsolved H_2O per unit volume of melt is calculated using

$$n_{e,i} = n - n_{d,i} \,. \qquad \text{Eq. A7}$$

This allows ϕ_i to be calculated (Eqs. A4 and A6), hence Δp_i (Eq. A1). This is repeated down the stack of layers. At some depth $n_{d,i} \geq n$, indicating that there is no exsolved gas phase, hence $\phi = 0$ for this and all subsequent layers.

Example calculation:

Assume the vesicularity of the top layer $\phi_1 = 0.7$ and ambient pressure $p_0 = 10^5$ Pa. We take $\rho = 2750$ kg/m3 for a typical Kīlauea basaltic melt, based on Lesher and Spera (2015), and $T = 1423$ K, which is a typical eruption temperature for Kīlauea basalt. From Eq. A2 we have $p_1 = p_0$ and from Eq. A3 we have $C_1 = 0.07714$ wt.%, giving $n_{d,1} = 117.85$ mol/m3 from Eq. A5. From Eq. A4 we have $\rho_{g,1} = 0.1521$ kg/m3, giving $n_{e,1} = 19.72$ mol/m3 from Eq. A6, hence $n = 137.6$ mol/m3. If we further assume a layer thickness of 0.01 m, the contribution to the hydrostatic pressure arising from layer 1 is $\Delta p_1 = 80.93$ Pa.

From Eq. A2, we can calculate the pressure on layer 2, $p_2 = 10{,}081$ Pa, hence the solubility $C_2 = 0.07717$ wt.% (Eq. A3) giving $n_{d,2} = 117.91$ mol/m3 from Eq. A5 and $n_{e,2} = 19.67$ mol/m3 from Eq. A7. The density of the gas $\rho_{g,2} = 0.1523$ kg/m3 from Eq. A4 hence, by rearranging Eq. A6, we obtain the vesicularity $\phi_2 = 0.6993$. Finally, from Eq. A1 we find $\Delta p_2 = 81.13$ Pa. Continuing in the same manner down the layers, we obtain the vesicularity profile presented in Figure A1.

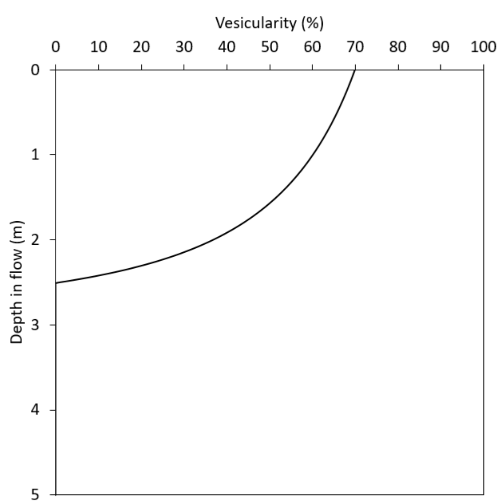

Figure A1. Computed vesicularity profile computed for a lava with surface vesicularity $\phi = 0.7$ (i.e. 70 % vesicular). Note that the combined effect of increasing solubility and increasing gas density with depth leads to fully dense lava (i.e. $\phi = 0$) below a depth of 2.5 m.

References

Iacono-Marziano, G., Morizet, Y., Le Trong, E. and Gaillard, F., 2012, New experimental data and semi-empirical parameterization of H2O–CO2 solubility in mafic melts. Geochimica et Cosmochimica Acta, 97, p.1–23. [https://doi.org/10.1016/j.gca.2012.08.035]

Lesher, C.E. and Spera, F.J., 2015, Thermodynamic and transport properties of silicate melts and magma. In: Sigurdsson, H., Houghton, B., Rymer, H., Stix, J., and McNutt, S., editors, The Encyclopedia of Volcanoes (Second Edition), Elsevier, p. 113–141. [https://doi.org/10.1016/B978-0-12-385938-9.00005-5]